Researchers Journal of Science and Technology (REJOST)

https://rejost.com.ng

Integrated Log-Derived Geomechanical Characterization and Sand Production Prediction for Sand Management in the EL Field, Niger Delta

Etim, Camillus Eyo, Bassey Nsikak Edet, Thomas Akpan Harry & Ekefre, Anyanime Edet

Abstract

Sand production remains a persistent operational challenge in weakly consolidated clastic reservoirs of the Niger Delta, often leading to wellbore instability, equipment erosion, and premature well abandonment. Despite numerous sanding studies in the basin, many rely on single-parameter or empirical approaches that do not fully integrate reservoir geomechanics, stress evolution, drawdown effects, and completion design within a unified workflow. This study presents an integrated, log-derived geomechanical characterisation of reservoirs in the EL Field, Niger Delta, with the objective of predicting sand production risk and optimising sand control strategies. Four reservoirs (K7.1, L9.1, M1.0, and M3.0) were analysed using wireline log-derived elastic properties, empirical rock strength correlations, in-situ stress modelling, sand production indices (SPI), and critical drawdown pressure (CDP) analysis. In addition, perforation orientation effects and sieve-based grain size analysis were incorporated to guide completion design. The reservoirs exhibit average elastic properties of Poisson's ratio 0.31, Young's modulus 2.52 Mpsi, shear modulus 0.97 Mpsi, bulk modulus 2.13 Mpsi, and Biot's coefficient 0.58. Rock strength analysis indicates a mean unconfined compressive strength of 5,672 psi, with the M-series reservoirs showing higher strength and stiffness than the shallower K7.1 and L9.1 units. The in-situ stress regime is dominated by normal faulting ($\sigma v > SHmax > Shmin$), consistent with the regional Niger Delta stress framework. Sand production prediction results show that K7.1 and L9.1 are highly sanding-prone, while M1.0 and M3.0 exhibit moderate to low sanding tendencies. CDP analysis further demonstrates that shallow reservoirs fail at relatively low drawdowns, whereas deeper reservoirs can sustain higher drawdowns but may release larger sand volumes upon failure. Based on integrated geomechanical and sieve analysis results, gravel pack completions are recommended for

K7.1, L9.1, and M1.0, while a standalone wire-wrapped screen is suitable for M3.0. The study demonstrates that integrating log-derived geomechanics, sanding indices, CDP, perforation orientation, and grain size analysis provides a robust and transferable workflow for sand management in Niger Delta reservoirs.

✉ Etim, Camillus Eyo: kamillusetim@gmail.com; camillusetim@aksu.edu.ng

Department of Geology, Akwa Ibom State University, Mkpat Enin, Uyo, PMB 1162, Nigeria

Keywords: Geomechanical characterization; In-situ stress; Critical drawdown pressure; Sanding prediction; Perforation orientation

Article history
Received: October 29, 2025
Received in revised form: December 21, 2025
Accepted for publication: December 30, 2025
Available online: January 3, 2026

1.0 Introduction

Sand production remains one of the most critical operational challenges in hydrocarbon exploitation, particularly in reservoirs composed of weakly consolidated or unconsolidated formations. This phenomenon is widespread across global oil and gas provinces and poses significant threats to production efficiency, operational safety, and project economics (Morita et al., 1989a; Sayers & Zoback, 2023). In the Niger Delta Basin, the risk of sand production is especially high due to its geological framework, which is dominated by young, poorly lithified clastic sediments (Adeyanju & Oyekunle, 2020). Several mature producing assets within the basin, including the EL Field, have experienced persistent sand influx during production, leading to frequent mechanical equipment failures, reduced production rates, increased operating costs, and in extreme cases, premature well abandonment (Oladapo et al., 2024). If not effectively managed, sand production can result in severe reservoir impairment, wellbore instability, erosion of tubing and surface facilities, and ultimately complete well failure (Adewole et al., 2023).

Sand production is governed by a complex interaction between reservoir geomechanical properties, in-situ stress conditions, and production-induced stress changes. Mechanistically, sanding initiates when hydrodynamic drag forces exerted by produced fluids exceed the combined cohesive strength and confining stresses of the formation, causing sand grains to detach from the rock matrix and migrate into the wellbore (Osisanya, 2021). The onset and severity of sand production are strongly influenced by rock mechanical parameters such as uniaxial compressive strength (UCS), tensile strength, Young’s modulus, Poisson’s ratio, and formation cohesion (Santarelli et al., 2020; Fjær et al., 2023). Progressive reservoir depletion further modifies the effective stress path, potentially triggering sand failure in intervals that were initially stable under pre-production conditions (Zhang, 2013a; Nwozor et al., 2024). As a result, a comprehensive understanding of the geomechanical behaviour of the EL Field reservoir is essential for reliable sand production prediction and mitigation.

Numerous sand control technologies including gravel packing, chemical consolidation, wire-wrapped screens, and expandable sand screens have been developed to mitigate sand-related challenges in unconsolidated reservoirs. However, the selection, design, and long-term effectiveness of these techniques are strongly dependent on reservoir geomechanical conditions (Ding et al., 2018; Khaksar et al., 2024). An optimal sand control strategy therefore requires an integrated geomechanical framework that incorporates rock mechanical characterization, in-situ stress evaluation, and production dynamics (Plumb et al., 2000; Fjær et al., 2023). Traditional empirical sanding prediction approaches, while widely applied, are often limited by their inability to capture the dynamic evolution of reservoir conditions such as pressure drawdown, increasing water cut, and stress redistribution (Adeyanju & Oyekunle, 2020). Recent advances in numerical and finite element modelling techniques provide more robust, physics-based tools for evaluating sanding mechanisms and optimizing sand control design under changing reservoir conditions (Schutjens et al., 2023; Chen et al., 2024).

Despite extensive research on sand production in the Niger Delta, relatively few studies have adopted an integrated workflow that combines elastic and strength properties derived from wireline logs with in-situ stress analysis, multiple sand production indices, critical drawdown pressure modelling, perforation orientation assessment, and grain size distribution analysis to directly inform field-scale sand management decisions (Afolayan et al., 2024; Abdideh et al., 2023). This limitation reduces the predictive reliability of sanding assessments and constrains the optimization of completion strategies, particularly in mature or marginal fields where operational margins are narrow (Oladapo et al., 2024).

This study addresses this gap by developing an integrated, log-derived geomechanical workflow for sand production prediction and sand control optimization in the EL Field, Niger Delta. Specifically, the study aims to: (i) estimate reservoir elastic and strength properties from wireline log data (Plumb et al., 2000; Eze et al., 2023); (ii) evaluate the in-situ stress regime and pore pressure conditions (Fjær et al., 2023; Sayers & Zoback, 2023); (iii) assess sanding potential using multiple elastic-based sanding indices and critical drawdown pressure analysis (Morita et al., 1989b; Osisanya & Ojo, 2023; Adewole et al., 2023); (iv) investigate the influence of perforation orientation on sanding risk (Wang et al., 2024; Udegbunam et al., 2025); and (v) recommend optimal sand control techniques based on sieve analysis of reservoir cuttings (Van den Hoek & Geilikman, 2023; Khaksar et al., 2024). The proposed integrated approach provides a practical and transferable framework for effective sand management in Niger Delta reservoirs and other similar clastic depositional environments worldwide.

2.0 Location and Geology of the Study Area

The study area is located in Southwest Niger Delta (Figure 1) in the Greater Ughelli depobelt. Figure 2 below is the base concession map showing well location and trajectory. The tectonic evolution of the Niger Delta is fundamentally linked to the Early Cretaceous opening of the South Atlantic Ocean, following the separation of the African and South American plates. This breakup led to the development of intracontinental rift systems across West Africa, including the Benue Trough, Abakaliki Rift, and Dahomey Basin, which were dominated by extensional tectonics and NE–SW trending normal faults that later influenced sedimentation and structural styles in the Niger Delta (Genik, 1993).

By the Late Cretaceous–Paleocene, seafloor spreading had established a passive continental margin characterized by thermal subsidence and tectonic quiescence. During this phase, thick marine sediments of the Akata Formation were deposited in deep-water environments, forming over-pressured shales that constitute the main hydrocarbon source rock of the basin (Reijers, 2011).

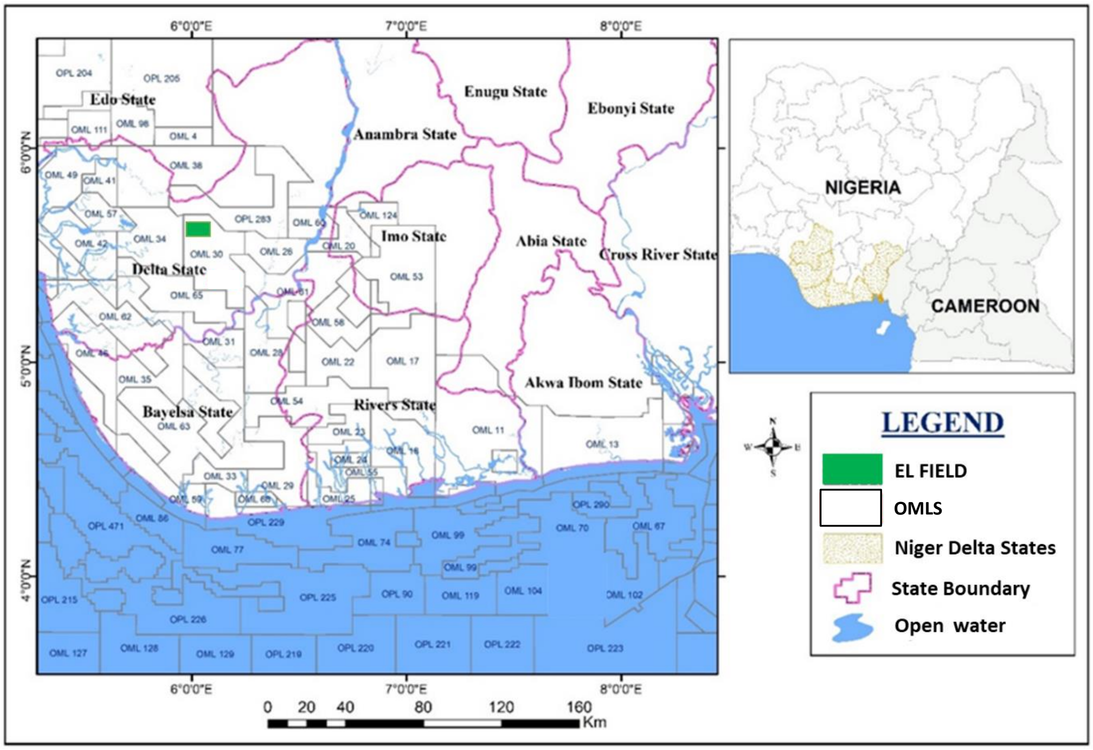

Figure 1: Map of Niger Delta showing the study area

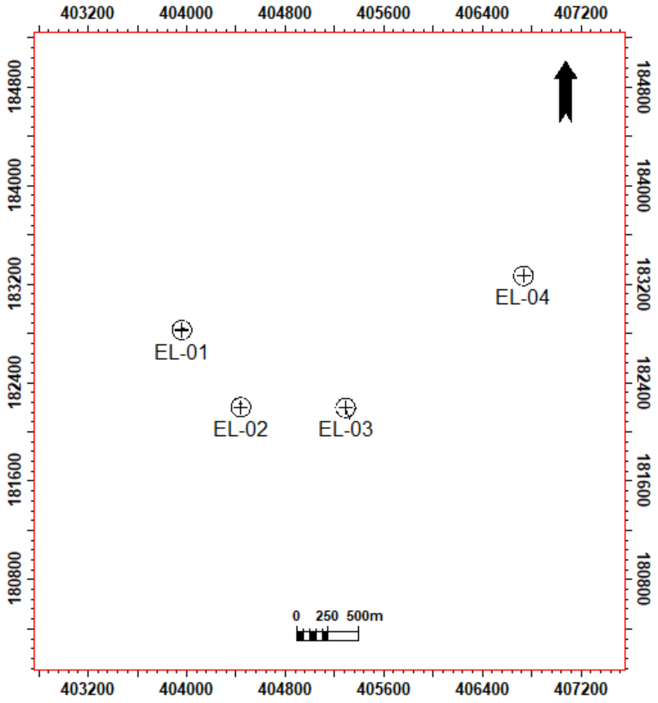

Figure 2: Base map of the study area showing well locations

Delta progradation began in the Eocene with the influx of large volumes of clastic sediments from the Niger River system, marking the transition from marine to deltaic sedimentation. The depositional system evolved from wave-dominated to fluvially dominated as sediment supply increased (Short & Stauble, 1967). Rapid sediment loading on the ductile Akata Shale triggered gravity-driven tectonics, resulting in listric growth faults, rollover anticlines, shale diapirs, and toe-thrust structures that are critical to hydrocarbon trapping (Doust & Omatsola, 1990).

Structurally, the Niger Delta is divided into extensional, transitional, and compressional tectonic provinces. The extensional province on the shelf is dominated by listric normal faults and rollover structures, while the transitional and compressional provinces exhibit detachment zones, shale ridges, toe-thrusts, and imbricate thrust systems formed by gravitational collapse of the sedimentary wedge (Evamy et al., 1978; Morley, 2009).

Despite its passive margin setting, the tectonic framework of the Niger Delta has been strongly influenced by inherited basement structures, including the Chain and Romanche Fracture Zones and Pan-African lineaments. These structures-controlled fault orientations, depocenter development, and sediment dispersal patterns, playing a key role in petroleum system distribution and trap geometry (Whiteman, 1982; Damuth, 1994).

The EL Field is located in the onshore Niger Delta and is hosted within the Agbada Formation, the basin's primary reservoir unit. The formation comprises interbedded sandstones and shales deposited in fluvial to shallow marine environments during delta progradation. In the EL Field, hydrocarbon-bearing reservoirs occur at depths between approximately 6,000 ft and 10,000 ft and are structurally controlled by growth fault systems typical of the extensional province. These faults facilitate hydrocarbon migration from the underlying Akata Formation and form structural traps in combination with rollover anticlines, while interbedded shales provide effective seals.

Overall, the Niger Delta represents a structurally complex, gravity-driven deltaic system shaped by continental rifting, passive margin development, and sustained sediment loading. Within this framework, the EL Field exemplifies a typical onshore Agbada Formation reservoir where tectonic structures exert strong control on reservoir architecture, hydrocarbon trapping, and production behavior, underscoring the importance of tectonic understanding for effective field development.

3.0 Materials and Methods

The study utilized conventional wireline log data acquired from wells in the EL Field, Niger Delta. The available logs include gamma ray, density, compressional sonic, neutron porosity, resistivity logs, etc. Prior to analysis, all logs were quality checked, depth matched, and environmentally corrected to minimize borehole and tool related effects. Shale intervals were identified using the gamma ray log, while clean reservoir sands were delineated based on low gamma ray response and consistent porosity trends. Only high-quality log intervals within the identified reservoir units were used for geomechanical computations. Detailed data availability is given in Table 1.

Table 1: Well Inventory

Wells	Cali	RhoB	DT	GR	Perf.	SP	RES	SW	VSH	PHI
EL 1	🟩	🟥	🟥	🟩	🟩	🟩	🟩	🟩	🟥	🟩
EL 2	🟩	🟩	🟩	🟩	🟩	🟥	🟩	🟩	🟩	🟩
EL 3	🟩	🟩	🟩	🟩	🟩	🟩	🟩	🟩	🟥	🟩
EL 4	🟩	🟩	🟥	🟩	🟩	🟩	🟩	🟩	🟥	🟩

Present	🟩
Absent	🟥

Cali – Caliper, RhoB – Bulk Density, DT – Sonic, GR - Gamma, Perf. – Perforation interval, SP – Spontaneous potential, RES – Resistivity, SW – Water Saturation, VSH - Volumes of Shale, PHI - Porosity

In addition, the data were analyzed and interpreted using the following software: Schlumberger Petrel, interactive petrophysics, and Microsoft Excel. Elastic properties were derived from compressional sonic and density logs. In details, compressional velocity (*Vp*) was obtained from the compressional transit time log, while shear velocity (*Vs*) was estimated using an empirical *Vp–Vs* relationship appropriate for unconsolidated to weakly consolidated sandstones as described in detail by Eshkalk *et al*. (2014); Azizi and Memarian (2015) in equations 1 and 2.

$$V_p = 357.346 \text{ x } \rho^4 \qquad (1)$$

where 357.346 is Gardner coefficient and ρ is density.

$$\text{V}_s = 0.802V_p - 0.8559 \qquad (2)$$

From the above equations, dynamic elastic moduli, including Young's modulus, shear modulus, bulk modulus, and Poisson's ratio, were computed using standard elastic relationships. However, the log derived Poisson ratio was computed using V_p and V_s relationship given in equation 3.

$$\text{Poisson's ratio } (\nu) = \frac{V_p^2 - 2V_s^2}{[2(V_p^2 - V_s^2]} \qquad (3)$$

The theoretical maximum value of v = 0.5. Dynamic Young's Modulus (*E*) was estimated using density, *Vp* and *Vs* relationship expressed in equation 4; shear modulus (*G*) was calculated using equation 5 (Omar, 2015) and bulk modulus (K_b) was estimated using the formula expressed in equation 6.

$$E = \frac{\left(\rho Vs^2 \times \left(3V_p{}^2 - 4V_s{}^2\right)\right)}{V_p{}^2 - V_s{}^2} \qquad (4)$$

where E = Young's modulus and ρ = bulk density.

$$G = \rho V_s^2 \qquad (5)$$

$$K_b = \rho \frac{Vp^2 - 4}{3Vs^2} \qquad (6)$$

Using bulk modulus, bulk compressibility (C_b) was determined using equation 7 while Biot's constant was estimated using Schlumberger, 1985 method in equation 8.

$$C_b = \frac{1}{K_b} \qquad (7)$$

$$\alpha = 1 - \frac{K_b}{K_r} \qquad (8)$$

where α is the Biot constant and K_r is the solid grain moduli as expressed in equation 9.

$$K_r = KS_{pma} / \left({}^{1}/_{\Delta Tcma^2} - \frac{4}{3\Delta Tsma^2}\right) \qquad (9)$$

where KS is constant and is equal to 1000 for metric units and 13400 for English units.

For the determination of rock strength, Unconfined compressive strength (UCS) was determined using McNally (1999) relationship (equation 10).

$$UCS = 1200\, exp^{(-0.036\Delta T_c)} \qquad (10)$$

This relationship is specifically used for fine grained, consolidated and unconsolidated sandstones with all porosity ranges suitable for the Niger Delta. In situ rock's tensile strength (T_o) was determined using the empirical relationships by Abijah and Tse, 2020 (equation 11)

$$T_o = \frac{C_o}{12} \qquad (11)$$

where cohesive strength (Co) was estimated using Mohr-Columb failure criterion (equation 12). Given the frictional angle (φ) in the equation, it was estimated using the model by Khaksar *et al*., 2009 (equation 13).

$$Co = \frac{UCS}{2\tan\,(45^o + (\frac{\varphi}{2})} \qquad (12)$$

$$\varphi = sin^{-1}((\frac{304878}{\Delta t_c} - 1000)/(\frac{304878}{\Delta t_c} + 1000) \qquad (13)$$

For the determination of in situ stresses, the overburden stress or vertical stress was computed as an integral of the rock density to the depth of interest from density log using equation (14) cited by Jones *et al*. (1992).

$$\sigma_v = \rho g \int_0^h dh = \rho g h \tag{14}$$

For onshore, the vertical or overburden stress is calculated by the expression given by Omar (2015) in equation 15.

$$\sigma_v = \rho \times 1000 \times g \times h \times 0.3048 \times 0.000145037738 \tag{15}$$

where σ_v is the vertical stress; ρ is the formation bulk density read off from density log, g is acceleration due to gravity and h is the depth of interest, 1000 converts density from g/cm³ to kg/m³, 0.3048 converts depth from feet to meters and 0.000145037738 converts pressure from Pascals (Pa) to psi. The minimum horizontal stress was estimated using elastic uniaxial strain model proposed by Ahmed et al. (1991). The model assumes zero lateral strain and elastic deformation of the formation. Under this condition, the minimum horizontal stress is expressed as a function of overburden stress, pore pressure and Poisson's ration as in equation 16.

$$S_{hmin} = \frac{v}{(1-v)}\left(\sigma_v - \alpha P_p\right) + \alpha P_p \tag{16}$$

where σ_v is the overburden stress, ν is the Poisson's ratio, P_P is the pore pressure, α is the Biot's constant and Sh_{min} is the minimum horizontal stress. Furthermore, the estimation of the magnitudes of the major and minor principal stresses (i.e. maximum and horizontal) were calculated from using a poroelastic model (Holbrook & Maggiori, 1993; Ostadhassan *et al*., 2012) in equation 17.

$$S_{Hmax} = \frac{\nu}{\left(1-\nu^2\right)}\left(\sigma_v - \alpha P_p\right) + \alpha P_p + \frac{E_{stat}}{\left(1-\nu^2\right)}\varepsilon_y + \nu\varepsilon_x \tag{17}$$

where S_{Hmax} is maximum horizontal stress, ν is Poisson's ratio, σ_v is the vertical or overburden stress, P_P is pore pressure, α is Biot constant, E_{stat} is the static Young's moduli, E_x and E_y are strain at maximum and minimum horizontal stress directions (Maleki *et al*., 2014). The deformation (strain) in the maximum and minimum horizontal directions is given by (Kidambi and Kumar, 2016) in equation 18 and 19 as:

$$\varepsilon_x = \frac{\sigma_v \times v}{E_{stat}} \times \left(\frac{1}{1-v} - 1\right) \tag{18}$$

$$\varepsilon_y = \frac{\sigma_v \times v}{E_{stat}} \times \left(1 - \frac{v^2}{1-v}\right) \tag{19}$$

To obtain the Young's modulus static constant from the dynamic constant, the dynamic moduli must be converted using the relation established by (Seyed & Aghighi, 2015) expressed in equation 20 as:

$$E_{stat} = 0.731 \times E_{dyn} - 2.337 \tag{20}$$

where 0.731 and 2.337 are Seyed and Aghighi constants obtained from laboratory experiment on core and applied for static correction of elastic constant. Pore pressure was further computed using equation 21 as expressed by Jones *et al*., (1992) and (Omar, 2015) given the relationship below.

$$P_p = P_f g \int_0^h dh = P_f g h$$

Or

$$P_p = P_f \times 1000 \times \mathrm{g} \times \mathrm{h} \times 0.30348 \times 0.0001450378 \tag{21}$$

where, P_f = pore fluid density, g is the acceleration due to gravity, P_P is the pore pressure, h is the depth, 1000 converts density from g/cm³ to kg/m³, 0.3048 converts depth from feet to meters and 0.000145037738 converts pressure from Pascals (Pa) to psi.

Reservoir sand production potential was evaluated using elastic-based sanding indices and critical drawdown pressure (CDP) analysis. The sanding indices relate changes in effective stress and rock strength to the likelihood of grain detachment around the wellbore. Sand production prediction based on rock elastic properties utilized i. Shear

Modulus to Bulk Compressibility Ratio (J) as in equation 22. ii. Sand Production Index Method (B) which incorporates Young's modulus and Poisson's ratio (equation 23). iii. Schlumberger Sand Production Index Method (SI) estimated using equation 24.

$$J = \frac{G}{C_b} \tag{22}$$

where G is the Shear modulus and C_b is the Bulk compressibility.

$$B = \frac{E}{3\,(1-2v)} + \frac{4}{3}\,(\frac{E}{2\,(1+v)}) \tag{23}$$

where B is the sand production index, E is the Young's modulus and v is the Poisson's ratio.

$$SI = K_b \times G \tag{24}$$

Critical Drawdown Pressure (CDP) which represents the onset condition at which the formation rock around the wellbore fails mechanically, releasing unconsolidated grains into the wellbore (Morita *et al.*, 1989b; Zoback, 2010). This was done to determine the propensity of sanding in the studied reservoirs under drawdown conditions. To this end, Critical Bottomhole Flowing Pressure (CBHP) was first estimated using equation 25 then, equation 26 was derived.

$$CBHP = \frac{1}{2-A}[2v - (3S_{hmax} - S_{hmin} - UCS)] \tag{25}$$

where, $A\ is\ the\ poroelastic\ constant = \frac{\alpha(1-2v)}{1-v}$

Therefore,

$$CDP = P_P - CBHP \tag{26}$$

It is noteworthy that the drawdown Pressure is related to the production rate, and its critical value corresponds to conditions when sanding of the rock occurs.

For the selection of optimum sand control, four (4) sand cuttings from the representative reservoirs (K7.1; L9.1; M1.0 and M3.0), boiled water and detergent were employed for this analysis. The equipment used for the analysis includes a sieve shaker with standard sieves, a sieve brush, and a hot air oven. Firstly, the sample were prepared by placing the cuttings in a container and soaked in hot water together with detergent to remove oil (if any). After decanting the oil and water, samples were then dried in a hot air oven and checked to ensure that all the grains were disintegrated. Secondly, Particle size distribution (PSD) analysis was carried out by using the dry sieving method. The Laboratory test sieves were cleaned and then measured to record the empty weight of sieves. The sieves were then stacked in a sieve shaker from a coarser sieve at the top to finer at the bottom, keeping the pan at the bottom. The prepared sample was weighted using an electronic balance and was placed on the same in the topmost sieve stacked in a sieve shaker. The Sieve shaker was switched on, and the shaking time was adjusted to 15 minutes. After completing the shaking cycle, the sieve weight and the retained sample were measured, and the net weight of retained sample on each sieve was calculated. The weight of the sample retained on each sieve was divided by the weight of the sample taken before sieving, and the result was multiplied by 100 to get the weight percentage retained on each sieve. The sample weight retained on each sieve was added with the sample weight retained on the succeeding sieve to find out the cumulative weight of the sample for all the sieves. The cumulative weight retained on each sieve was divided by the total cumulative weight, and the result was multiplied by 100 to find out the cumulative weight percentage of all the sieves. Finally, the cumulative weight percentage was plotted against sieve size on a semi-log graph using Microsoft Excel.

In the distribution curve, a horizontal straight line was from coordinates of cumulative weight percentage (Y-axis) to intersect the curve, and from that point on the curve, a vertical straight line was drawn downward to cross the X-Axis to get D10 (10 percentile of formation grain size diameter). The same procedure was employed using 40, 50, 90, 95 coordinates of cumulative weight percentage (Y-axis) to determine D40, D50, D90, D95, respectively, for all the four sand samples.

The formulas and rules through which the Optimum Sand Control Technique and well completion parameters for a particular field can be determined are shown in Tables 2 – 4.

Table 2: Formulas (Oil and Natural Gas Corporation Limited, 2018)

Parameters	Formulas
Sorting coefficient (SC)	D10/ D95
Uniformity Coefficient (UC)	D40/ D90
Fines Content	2*(Weight of the sample before Sieving-Cumulative Weight of the ASTM Mesh No.400. For this study it was gotten at the bottom pan)

Table 3: Standard Gravel Sizes of US ASTM Mesh (Oil and Natural Gas Corporation Limited, 2018)

Gravel Size, U.S. Mesh	Size Range, inch
8/12	0.094-0.066
12/20	0.066-0.033
20/40	0.033-0.017
40/60	0.017-0.0098
50/70	0.012-0.0083

Table 4: Standard Rules for optimum completion type selection (Oil and Natural Gas Corporation Limited, 2018)

Sorting Coefficient, Uniformity Coefficients (UC) and fines content			
Sorting coefficient	**Uniformity coefficient**	**Fines content (%)**	**Completion Types**
SC <10	UC <3	<2%	SAS (wire wrapped screen)
	UC < 5	< 5%	Pre-packed/Premium Screen
S C <20	UC<5	< 5%	GP/HRWP
	UC>5	> 5%	Frac Pack
Selection Of Screen Slot Size			
Uniformity coefficient			**Screen slot size selection**
UC < 2.00			D50
UC~2.00			D40
UC > 2.0			D30
Selection Of Gravel and Screen Size for Gravel Pack			
Largest Gravel			8 x D50
Smallest Gravel			4 x D50
Screen slot size			0.5 x 4 x D50

4.0 Results

The elastic properties of the studied reservoirs were determined from dynamic correlations. The Poisson's ratio ranges between 0.29 and 0.34, while Young's modulus varies from 1.53 to 3.05 Mpsi. The shear modulus lies between 0.74 and 1.14 Mpsi, and the bulk modulus between 1.82 and 2.28 Mpsi. Biot's coefficient was estimated to be within the range of 0.54 to 0.63.

On a reservoir basis (see table 5a), the average Poisson's ratio, Young's modulus, Shear modulus, bulk modulus and Biot's coefficient respectively are as follows: Reservoir K7.1 (0.33, 1.96 Mpsi, 0.74 Mpsi, 1.82 Mpsi and 0.63); Reservoir L9.1 (0.32, 2.36 Mpsi, 0.90 Mpsi, 2.13 Mpsi and 0.58); Reservoir M1.0 (0.29, 2.92 Mpsi, 1.14 Mpsi, 2.28 Mpsi and 0.54); Reservoir M3.0 (0.29, 2.82 Mpsi, 1.09 Mpsi, 2.27 Mpsi and 0.55). Figure 3a and b present the well correlation panel for both shallow sigma reservoirs (K7.1) and deeper lima reservoirs (L9.1, M1.0 and M3.0) across all the wells. However, according to figure 4, these results clearly suggest that the M-series reservoirs, particularly M1.0 and M3.0, possess the highest elastic stiffness among the studied intervals.

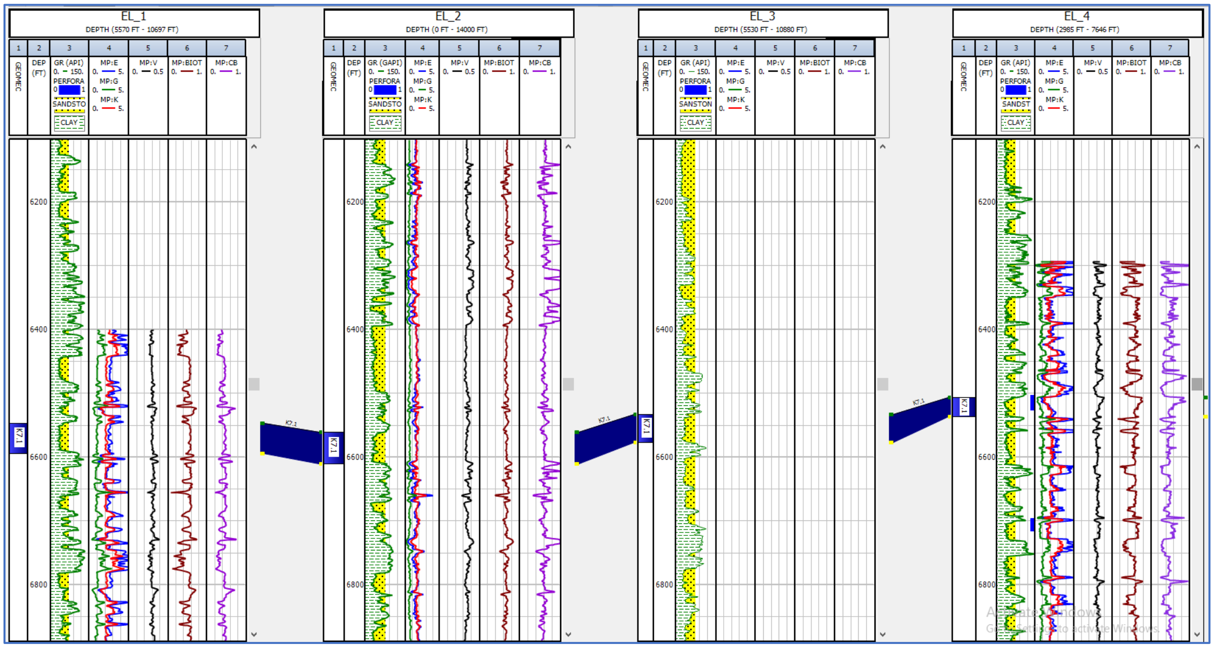

{Track 1- Gamma ray log; Track 2 – (Young modulus, shear modulus and bulk modulus); Track 3 – Poisson ratio; Track 4 – Biot coefficient; Track 5 – Bulk compressibility}

Figure 3a: Well correlation panel showing lateral variations in reservoir elastic properties for the shallow Lima Reservoir, illustrating stratigraphic continuity and heterogeneity across the correlated wells

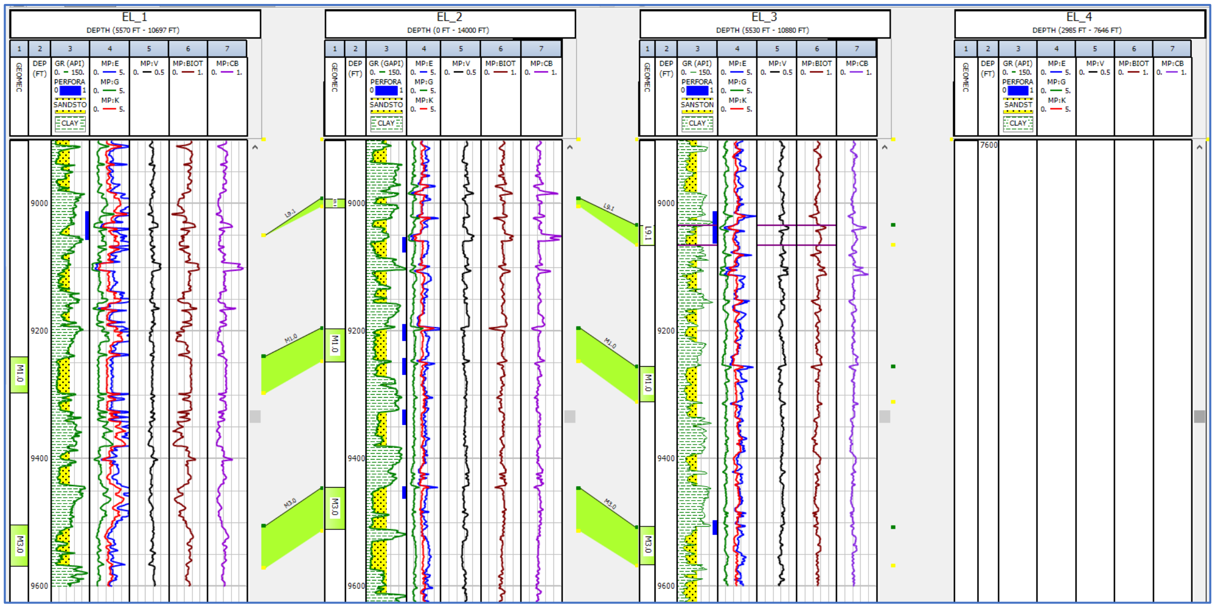

{Track 1- Gamma ray log; Track 2 – (Young modulus, shear modulus and bulk modulus); Track 3 – Poisson ratio; Track 4 – Biot coefficient; Track 5 – Bulk compressibility}

Figure 3b: Well correlation panel showing reservoir rock elastic properties for the deeper (Lima) Reservoirs

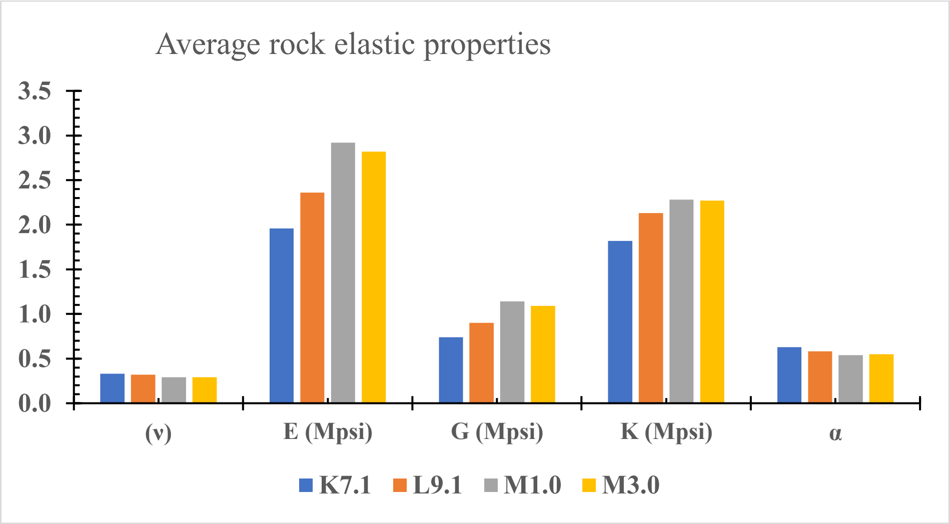

Figure 4: Histogram plot comparing the distribution of reservoir rock elastic properties across the four studied reservoirs, illustrating similarities and contrasts in their elastic behaviour.

Table 5a: Estimated reservoir rock elastic properties and rock strength

Reservoirs/wells			**Elastic properties**					**Rock strength**			
Res	**Wells**	**v**	**E (Mpsi)**	**G (Mpsi)**	**K (Mpsi)**	**CB (µsip)**	**α**	**UCS (psi)**	***To* (psi)**	**Co (psi)**	**ϕ (deg)**
K7.1	EL 1	0.3	2.62	1.01	2.19	0.46	0.56	4988.38	185.72	4553.4	32.44
	EL 2	0.34	1.53	0.57	1.58	0.64	0.68	3579.6	251.51	3018.13	28.37
	EL 3	-	-	-	-	-	-	-	-	-	-
	EL 4	0.34	1.73	0.65	1.69	0.62	0.66	4182.32	303.01	3636.14	29.1
	Mean	**0.33**	**1.96**	**0.74**	**1.82**	**0.57**	**0.63**	**4250.1**	**246.75**	**3735.89**	**29.97**
L9.1	EL 1	-	-	-	-	-	-	-	-	-	-
	EL 2	0.31	2.49	0.95	2.2	0.46	0.56	6196.67	469.39	5632.73	32.21
	EL 3	0.33	2.22	0.84	2.05	0.5	0.59	5142.49	382.24	4586.85	30.56
	EL 4	-	-	-	-	-	-	-	-	-	-
	Mean	**0.32**	**2.36**	**0.90**	**2.13**	**0.48**	**0.58**	**5669.58**	**425.82**	**5109.79**	**31.39**
M1.0	EL 1	0.29	2.75	1.07	2.17	0.46	0.57	5167.93	196.75	4692.58	32.63
	EL 2	0.29	2.96	1.15	2.3	0.44	0.54	7105.14	551.04	6612.47	33.16
	EL 3	0.29	3.05	1.19	2.38	0.42	0.52	7177.94	555.84	6670.03	33.3
	EL 4	-	-	-	-	-	-	-	-	-	-
	Mean	**0.29**	**2.92**	**1.14**	**2.28**	**0.44**	**0.54**	**6483.67**	**434.54**	**5991.69**	**33.03**
M3.0	EL 1	0.29	2.9	1.12	2.32	0.44	0.54	5548.28	247.2	5152.4	33.12
	EL 2	0.29	2.7	1.05	2.16	0.46	0.57	6433.23	489.47	5873.62	32.51
	EL 3	0.3	2.87	1.11	2.34	0.43	0.53	6871.54	528.51	6342.11	32.98
	EL 4	-	-	-	-	-	-	-	-	-	-
	Mean	**0.29**	**2.82**	**1.09**	**2.27**	**0.44**	**0.55**	**6284.35**	**421.73**	**5789.38**	**32.87**

Table 5b: Estimated reservoir rock insitu stresses and sand production indices

Reservoirs/wells		**Insitu Stresses**				**Sand Production Indices**		
Res	**Wells**	**σv (psi)**	**Shmin (psi)**	**SHmax (psi)**	**Pp (psi)**	**J ($Mpsi^2$)**	**B (Mpsi)**	**SI ($Mpsi^2$)**
K7.1	EL 1	6041	4739.74	5305.71	3210.64	2.22	2.43	2.22
	EL 2	6084	4915.54	5430.89	3572.27	0.93	1.42	0.93
	EL 3	-	-	-	-	-	-	-
	EL 4	6043.04	4924.8	5422.93	3675.75	1.2	2.56	1.2
	Mean	**6056.01**	**4860.03**	**5386.51**	**3486.22**	**1.45**	**2.14**	**1.45**
L9.1	EL 1	-	-	-	-	-	-	-
	EL 2	8571.3	6624.84	7633.34	4035.16	2.11	2.31	2.11
	EL 3	8457.92	6973.57	7657.71	4578.98	1.81	3.17	1.81
	EL 4	-	-	-	-	-	-	-
	Mean	**8514.61**	**6799.205**	**7645.53**	**4307.07**	**1.96**	**2.74**	**1.96**
M1.0	EL 1	8905.87	6853.98	7951.24	4161.52	2.32	2.56	2.32
	EL 2	8803.64	7030.38	7953.82	4608.71	2.73	2.75	2.73
	EL 3	8682.85	6988.87	7798.21	4285.38	2.85	3.96	2.85
	EL 4	-	-	-	-	-	-	-
	Mean	**8797.45**	**6957.74**	**7901.09**	**4351.87**	**2.63**	**3.09**	**2.63**
M3.0	EL 1	9194.89	7180.47	8274.56	4496.69	2.64	2.69	2.64
	EL 2	9073.5	7188.26	8190.22	4594.57	2.28	2.52	2.28
	EL 3	8930.23	7226.15	8050.69	4443.89	2.61	3.81	2.61
	EL 4	-	-	-	-	-	-	-
	Mean	**9066.21**	**7198.29**	**8171.82**	**4511.71**	**2.51**	**3.01**	**2.51**

The strength properties of the reservoir rocks were also evaluated, and the results demonstrate significant variations across the different reservoirs. However, from table 5a, the unconfined compressive strength (UCS) is approximately 4250 psi in K7.1, 5670 psi in L9.1, 6484 psi in M1.0 and 6284 psi in M3.0. Similarly, cohesion (Co) values are found to be about 3736 psi in K7.1, 5110 psi in L9.1, 5992 psi in M1.0 and 5789 psi in M3.0. Tensile strength (T_o) is lowest in K7.1 at about 247 psi, while L9.1, M1.0 and M3.0 exhibit values of 426 psi, 435 psi and 422 psi respectively. The friction angle increases from 30.0° in K7.1 to 31.4° in L9.1, 33.0° in M1.0 and 32.9° in M3.0. In this case, Figure 5a and b present the well correlation panel of these properties for both shallow sigma reservoirs (K7.1) and deeper lima reservoirs (L9.1, M1.0 and M3.0) across all the wells. Figure 6 graphically show the histogram plot of the estimated average values of the above properties reflecting its consistency with the result of the elastic properties of the studied reservoirs.

The magnitudes of the in-situ stresses and pore pressures were also estimated for each reservoir. Given table 5b, the vertical stress (σv) is about 6056 psi in K7.1, 8515 psi in L9.1, and 8797 psi in M1.0 and 9066 in M3.0. The minimum horizontal stress (Shmin) is approximately 4860 psi in K7.1, 6800 psi in L9.1 and 6958 psi in M1.0 and 7198 in M3.0, while the maximum horizontal stress (SHmax) is 5387 psi in K7.1, 7646 psi in L9.1 and 7901 psi in M1.0 and 8171 psi in M3.0. Pore pressures are appoximately 3486 psi in K7.1, 4307 psi in L9.1 and 4352 psi in M1.0 and 4551psi in M3.0. However, figures 7a and b present the well correlation panel of these properties for both shallow sigma reservoirs (K7.1) and deeper lima reservoirs (L9.1, M1.0 and M3.0) across all the wells. Figure 8 graphically show the histogram plot of the estimated average insitu stresses. From the plot, the deeper lima reservoir exhibits higher far field stresses.

Rock elastic property-based sanding indices (Table 5b) were calculated using the shear modulus to bulk compressibility Ratio (J), sand production index (B) and the Schlumberger Index (SI). The results show that the average value of J, B and SI respectively is 1.45 Mpsi^2, 2.14 Mpsi and 1.45 Mpsi^2 in K7.1 reservoir; 1.96 Mpsi^2, 2.14 Mpsi and 11.96 Mpsi^2 in L9.1 reservoir; 2.63 Mpsi^2, 3.09 Mpsi and 2.63 Mpsi^2 in M1.0 reservoir; 2.51 Mpsi^2, 3.01 Mpsi and 2.51 Mpsi^2 in M3.0 reservoir. Figure 9a and b present the well correlation panel of these properties for both shallow sigma reservoirs (K7.1) and deeper lima reservoirs (L9.1, M1.0 and M3.0) across all the wells. Figure 10 graphically show the histogram plot of the estimated averages of the sand production prediction indices and the comparison is consistent with other aforementioned properties.

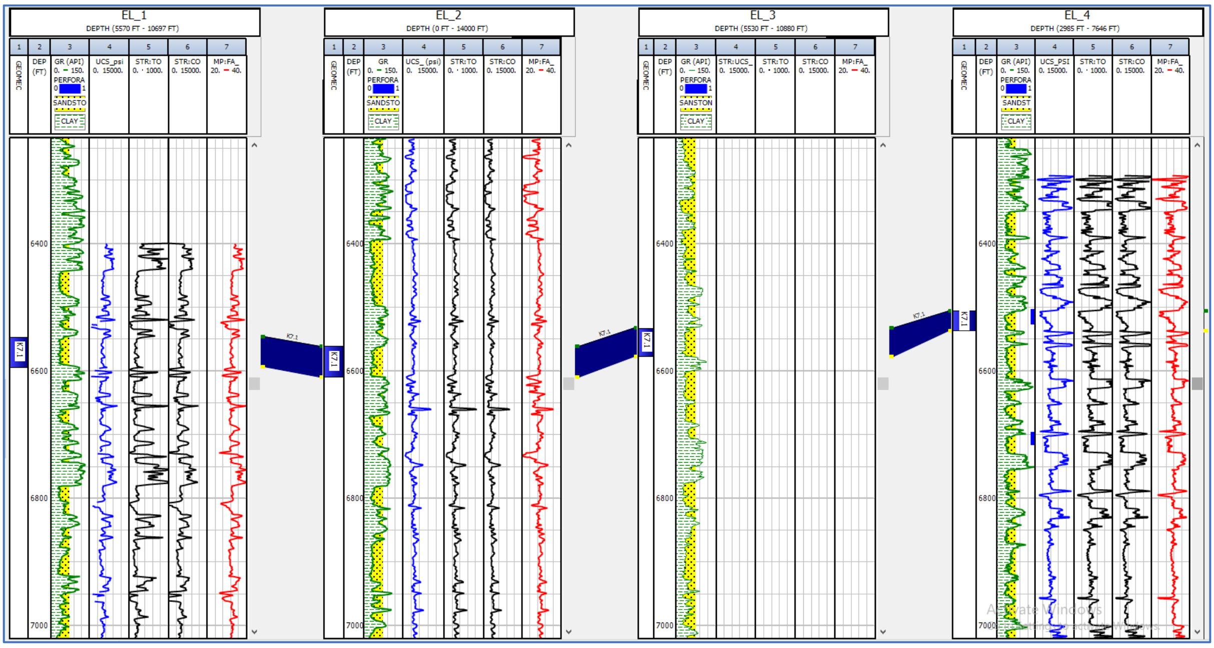

{Track 1- Gamma ray log; Track 2 – Unconfined Compressive Strength; Track 3 – Tensile strength; Track 4 – Cohesive strength; Track 5 – Frictional angle}

Figure 5a: Well correlation panel showing lateral variations in reservoir rock strength (Sigma), illustrating stratigraphic continuity and heterogeneity. Stronger intervals indicate more competent reservoir units, while weaker zones reflect less consolidated formations, with implications for reservoir quality and geomechanical stability.

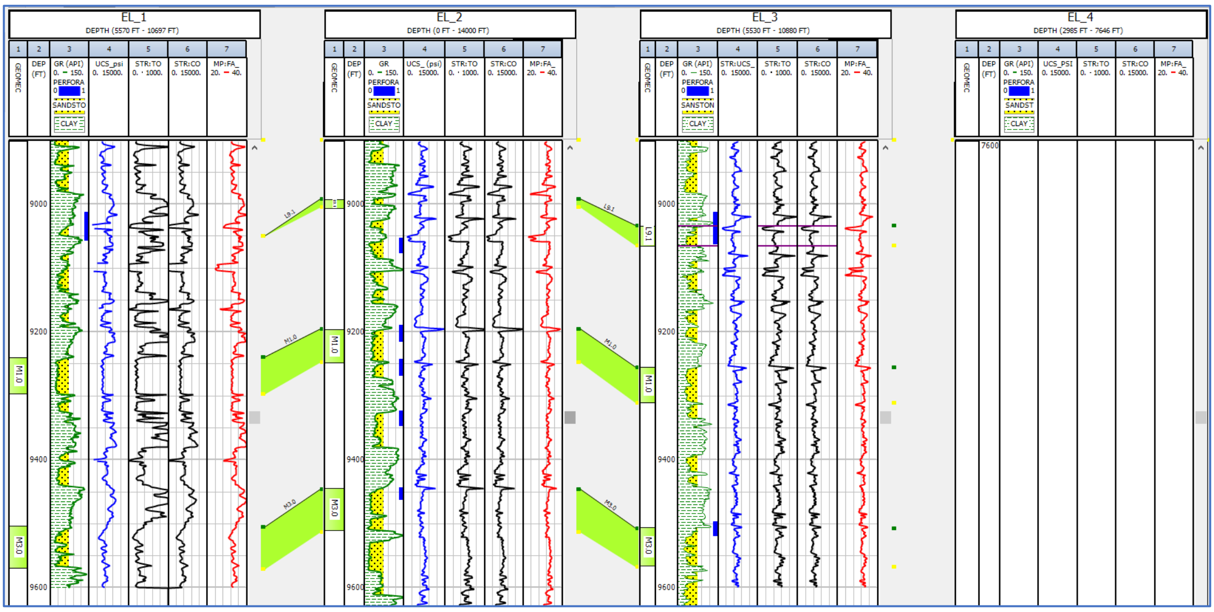

{Track 1- Gamma ray log; Track 2 – Unconfined Compressive Strength; Track 3 – Tensile strength; Track 4 – Cohesive strength; Track 5 – Frictional angle}

Figure 5b: Well correlation panel showing lateral variations in reservoir rock strength (Lima)

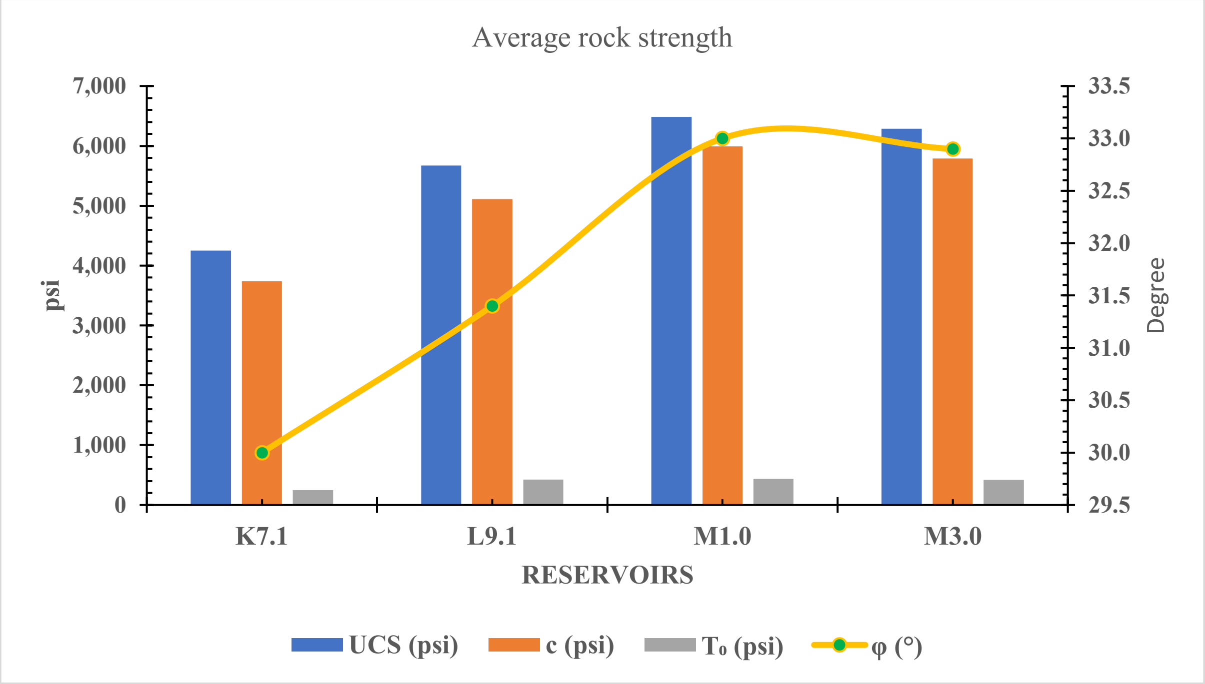

Figure 6: Histogram plot of reservoir rock strength

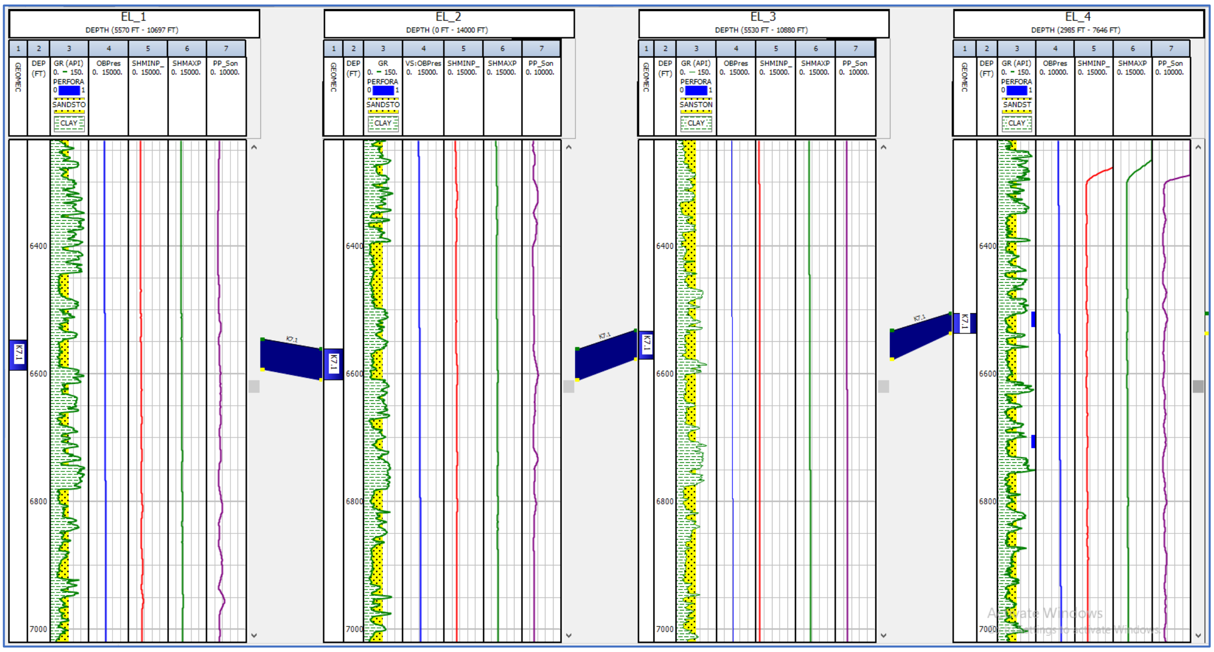

{Track 1- Gamma ray log; Track 2 – Vertical stress; Track 3 – Minimum horizontal stress; Track 4 – Maximum horizontal stress; Track 5 – Pore pressure}

Figure 7a: Well correlation panel (Sigma) illustrating lateral variations in reservoir in-situ stresses, demonstrating stress distribution and stratigraphic continuity across the correlated wells. Variations in stress magnitude reflect differences in lithology, depth, and mechanical properties, with implications for reservoir stability and wellbore integrity.

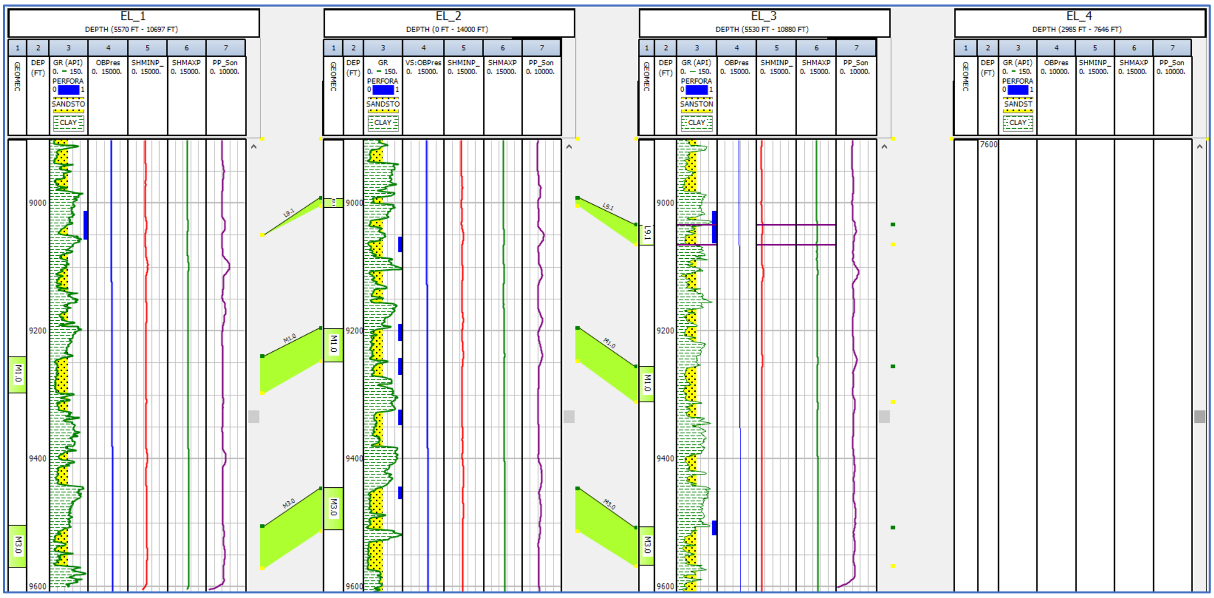

{Track 1- Gamma ray log; Track 2 – Vertical stress; Track 3 – Minimum horizontal stress; Track 4 – Maximum horizontal stress; Track 5 – Pore pressure}

Figure 7b: Well correlation panel showing reservoir insitu stresses (Lima)

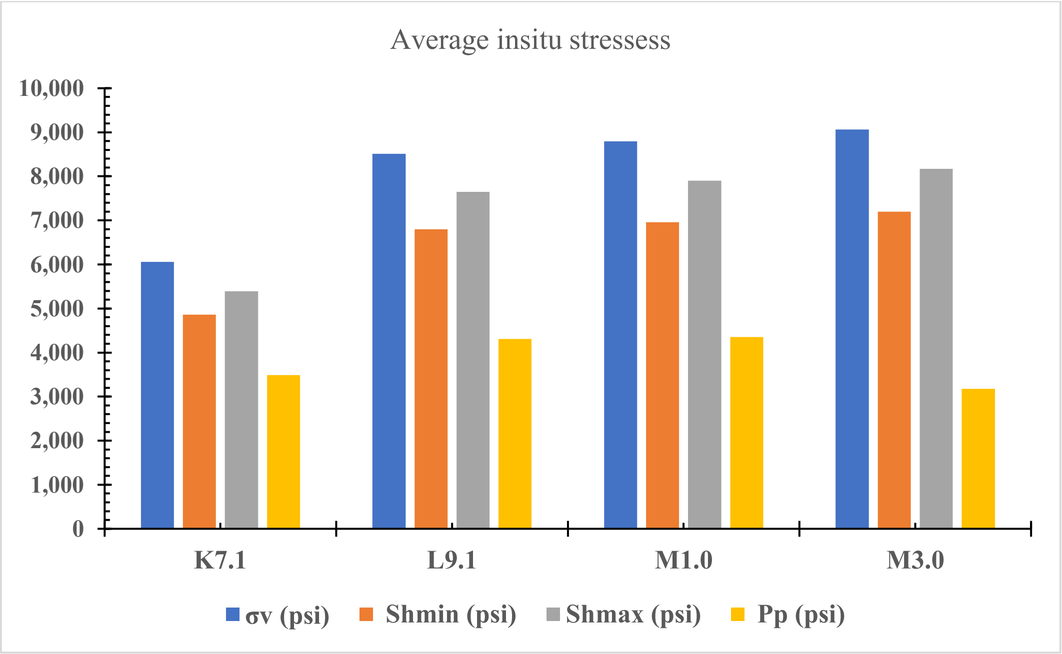

Figure 8: Histogram plot showing the distribution of reservoir in-situ stresses, illustrating variations in stress magnitude and frequency across the studied reservoir intervals

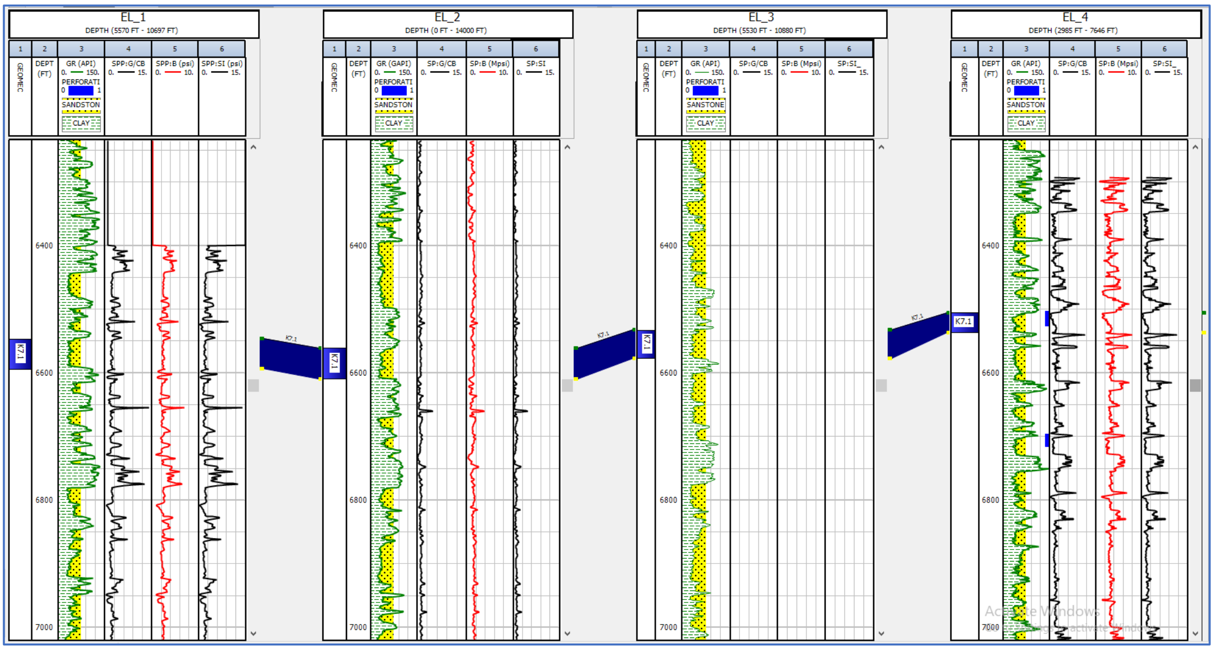

{Track 1- Gamma ray log; Track 2 – Shear modulus/Bulk compressibility ratio(G/CB); Track 3 – Sand production index (B); Track 4 – Schlumberger Sand production Index (SI)}

Figure 9a: Well correlation panel showing reservoir sand production indices (sigma)

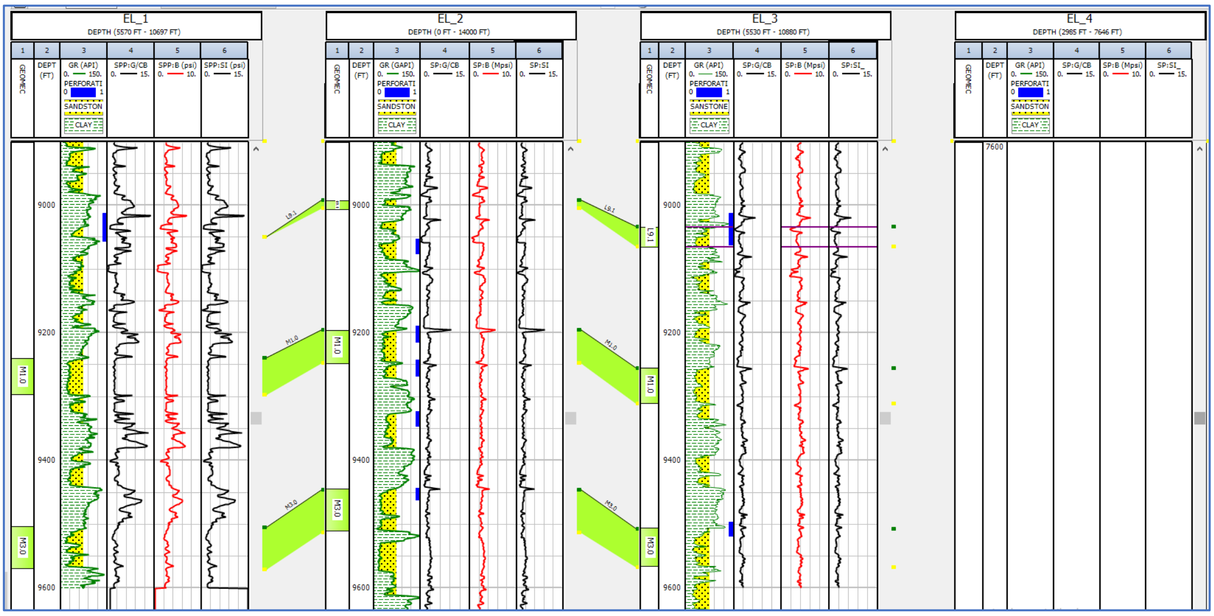

{Track 1- Gamma ray log; Track 2 – Shear modulus/Bulk compressibility ratio(G/CB); Track 3 – Sand production index (B); Track 4 – Schlumberger Sand production Index (SI)}

Figure 9b: Well correlation panel showing reservoir sand production indices (Lima)

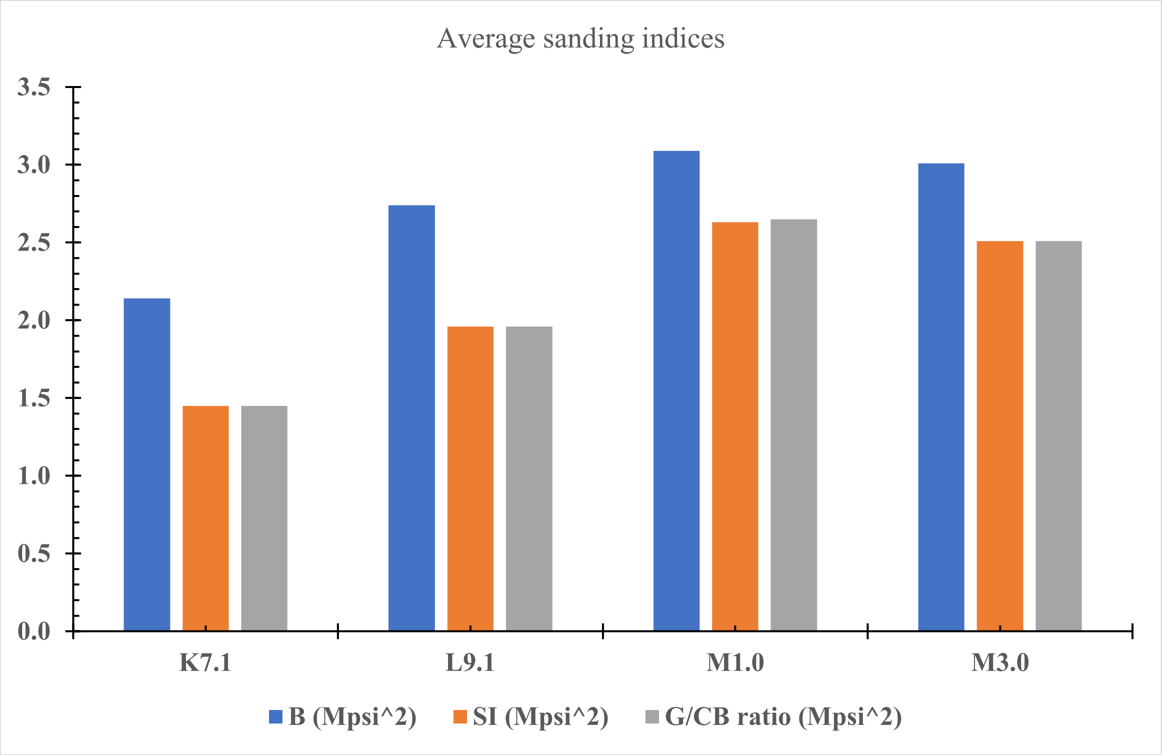

Figure 10: Histogram plot of reservoir sand production indices

The Critical Drawdown Pressure (CDP), Bottom Hole Flowing Pressure (BHFP), failure pressure and percentage reservoir pressure depletion were computed for perforation angles of 0°, 30°, 60° and 90° using shear failure model. These were done within the perforated interval corresponding to reservoir K7.1, L9.1, M1.0 and M3.0. However, at the center of this study was to determine the maximum drawdown before the onset of sand production.

Based on shear failure model for perforated well El_4 **(**Figure 12), the result of the discrete run at the perforated depth of 6514.5ft shows reservoir failure pressure at 0°, 30°, 60° and 90° perforation angles to occur at 2835psi, 2762psi, 2749psi and 2610psi respectively given the initial reservoir pressure of 4029 psi**.** The maximum allowable Bottomhole Flowing Pressure (BHFP) at perforation angles 0°, 30°, 60° and 90° before the onset of sand production are 2530 psi, 2381psi, 2355 psi and 2479psi respectively**.** Maximum drawdown before the onset of sand production or CDP are 604 psi, 753 psi, 778 psi and 655 psi corresponding to the four-perforation angle**.** However, from the BHFP and CDP values, the critical reservoir pressure before failure pressure is 3134 psi for all perforation angle. Figure 12 shows the histogram plot of percentage reservoir pressure depletion before the onset of sand production for reservoir K7.1. The plot shows that based on the perforation angle (0°, 30°, 60° and 90°), the percentage reservoir pressure is 29.64%, 31.45%, 31.77% and 35.22% respectively.

Also using the shear failure model for perforated well El_3 as illustrated in figure 13**,** simulations at a perforation depth of 9050 ft indicated that the reservoir would fail at pressures of 2041 psi, 1978 psi, 1851 psi, and 1787 psi for perforation angles of 0°, 30°, 60°, and 90°, respectively, compared with an initial reservoir pressure of 4479.78 psi**.** The corresponding maximum Bottomhole Flowing Pressures (BHFP) prior to sand initiation were 1799 psi at 0°, 1673 psi at 30°, 1416 psi at 60°, and 1741 psi at 90°. The Critical Drawdown Pressures (CDP) were determined as 477 psi, 604 psi, 861 psi, and 92 psi for the respective orientations. From the relationship between BHFP and CDP, the critical reservoir pressure before failure was found to be 2277 psi for the 0°, 30°, and 60° perforations, while for 90° it dropped to 1833 psi. As illustrated in **Figure 14,** the depletion analysis shows that sand onset occurred when reservoir pressure declines by 54.61%, 56.02%, 58.88%, and 60.26% for the 0°, 30°, 60°, and 90° perforation angles, respectively.

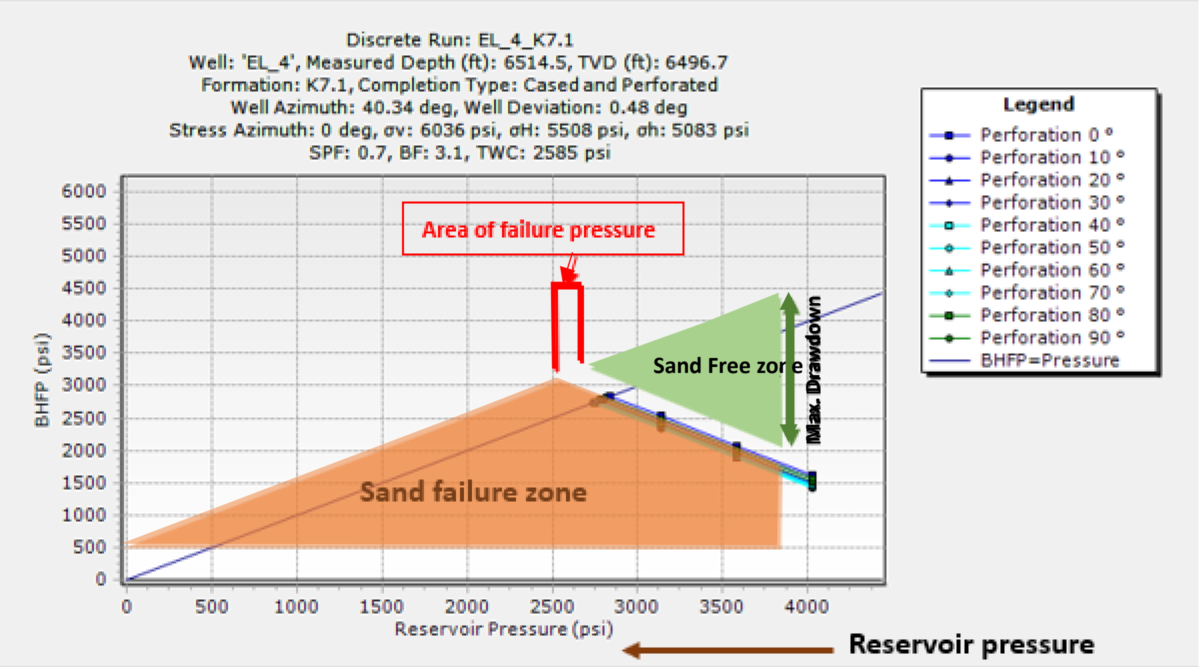

Figure 11: CDP prediction using shear failure model for perforated well EL 4 (Reservoir K7.1)

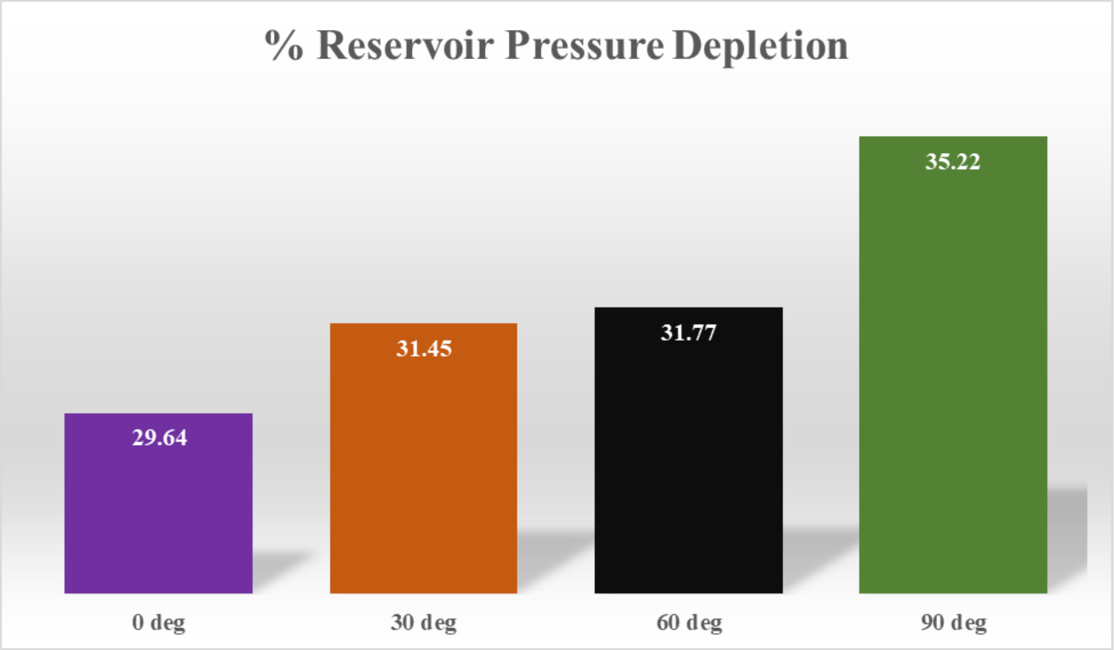

Figure 12: Histogram plot of percentage reservoir pressure depletion before the onset of sand production for Reservoir K7.1

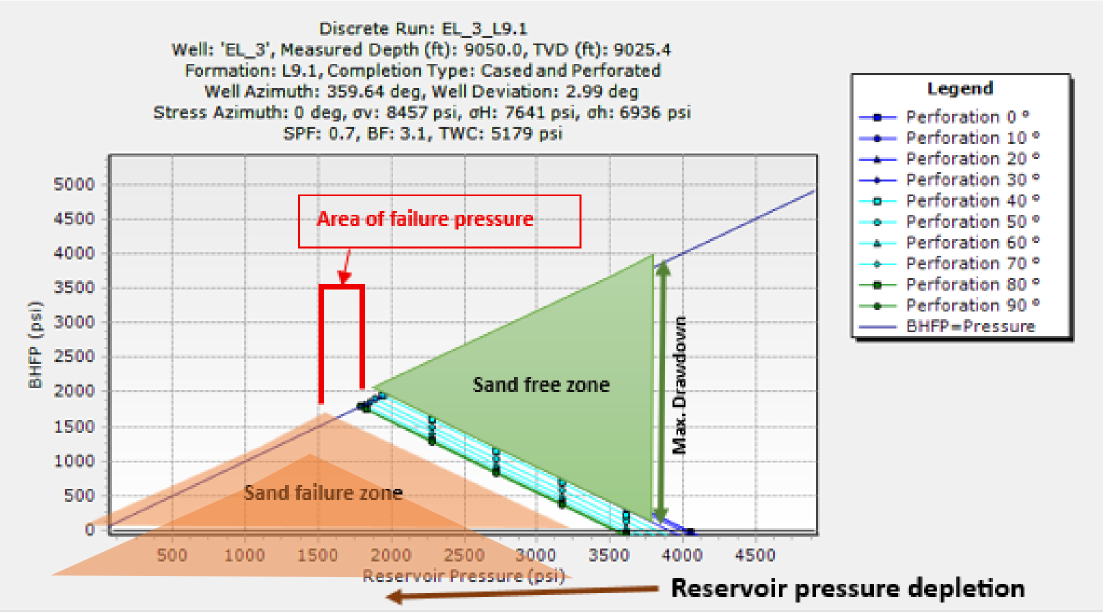

Figure 13: CDP prediction using shear failure model for perforated well EL 3 (Reservoir L9.1)

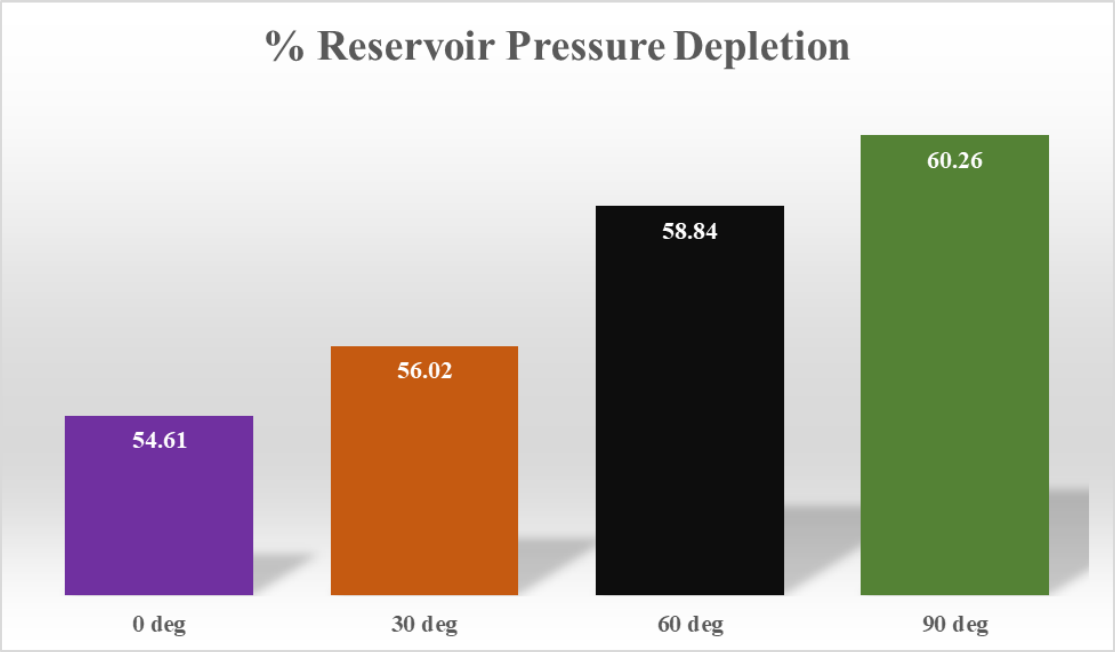

Figure 14: Histogram plot of percentage reservoir pressure depletion before the onset of sand production for Reservoir L9.1

Applying the shear failure model to perforated well El_1 (Figure 15)**,** analysis at a depth of 9260 ft revealed that reservoir failure occurred at pressures of 2265 psi, 2252 psi, 2072 psi, and 1905 psi for perforation angles of 0°, 30°, 60°, and 90°, respectively, relative to an initial reservoir pressure of 4204.47 psi**.** The corresponding maximum Bottomhole Flowing Pressures (BHFP) prior to sand initiation are 1964 psi, 1939 psi, 1997 psi, and 1658 psi for the respective angles. Critical Drawdown Pressures (CDP) calculated for the four cases are 594 psi, 619 psi, 150 psi, and 488 psi. From these results, the critical reservoir pressures before failure are identified as 2558 psi for the 0° and 30° orientations, and 2146 psi for 60° and 90°. As illustrated in Figure 16, the histogram of pressure depletion indicates that sand onset occurred after 46.13%, 46.44%, 50.72%, and 54.69% depletion for the 0°, 30°, 60°, and 90° perforation angles, respectively.

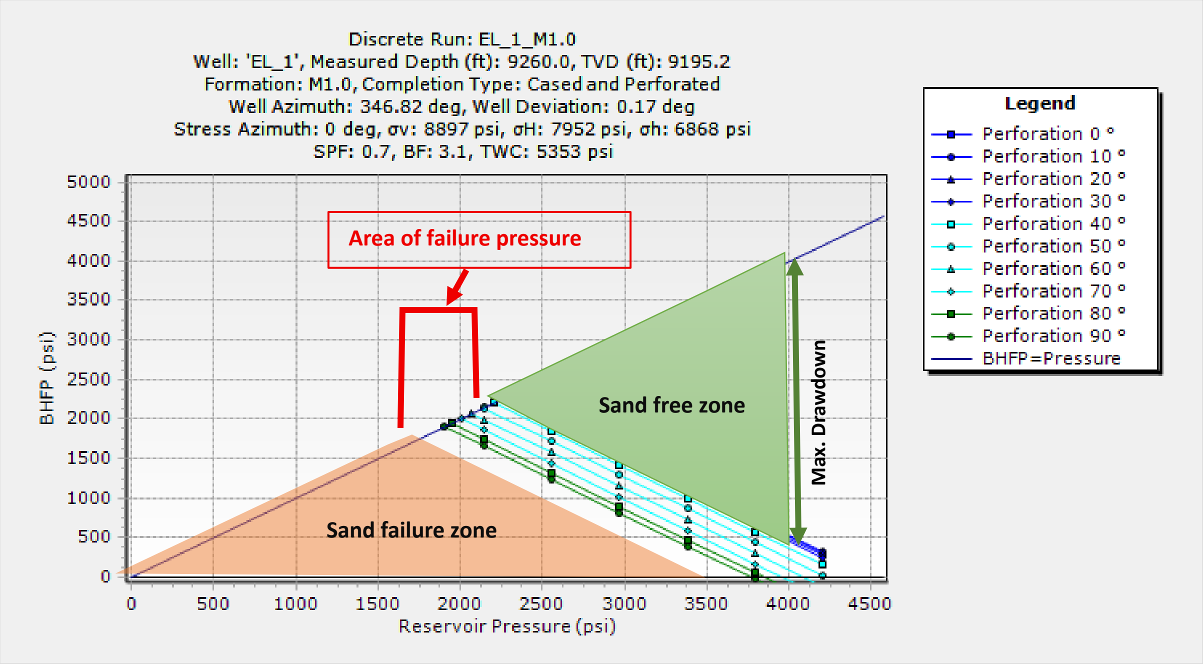

Figure 15: CDP prediction using shear failure model for perforated well EL 1 (Reservoir M1.0)

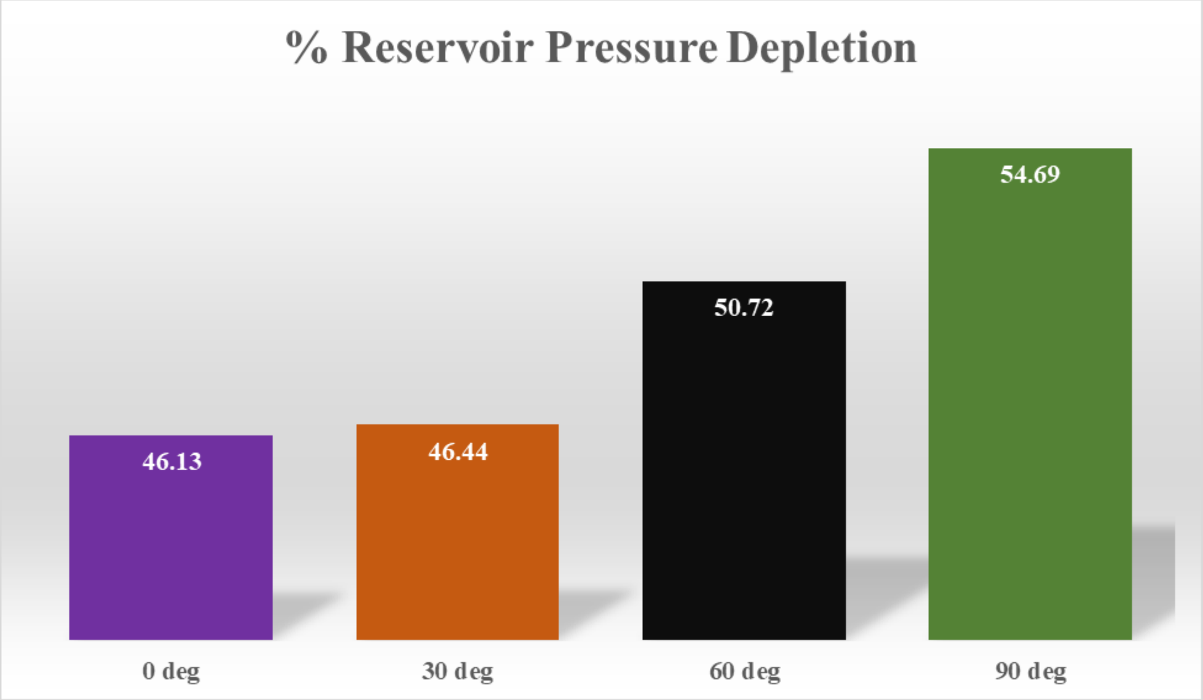

Figure 16: Histogram plot of percentage reservoir pressure depletion before the onset of sand production for Reservoir M1.0

Using the shear failure model for perforated well El_2 (Figure 17), simulation at a perforation depth of 9453 ft indicated reservoir failure pressures of 600 psi, 527 psi, 378 psi, and 301 psi at perforation angles of 0°, 30°, 60°, and 90°, respectively, compared to the initial reservoir pressure of 4385 psi. The corresponding maximum Bottomhole Flowing Pressures (BHFP) prior to sand onset are 218 psi, 70 psi, 265 psi, and 110 psi for the respective perforation angles. The calculated Critical Drawdown Pressures (CDP) are 757 psi, 905 psi, 222 psi, and 377 psi, showing variations with perforation orientation. From these BHFP and CDP values, the critical reservoir pressure prior to failure is estimated at 974 psi for 0° and 30°

perforations, and 487 psi for 60° and 90° perforations. As shown in Figure 18, the histogram illustrates percentage reservoir pressure depletion at sand onset, which was 86.32%, 87.98%, 91.38%, and 93.14% for perforation angles of 0°, 30°, 60°, and 90°, respectively.

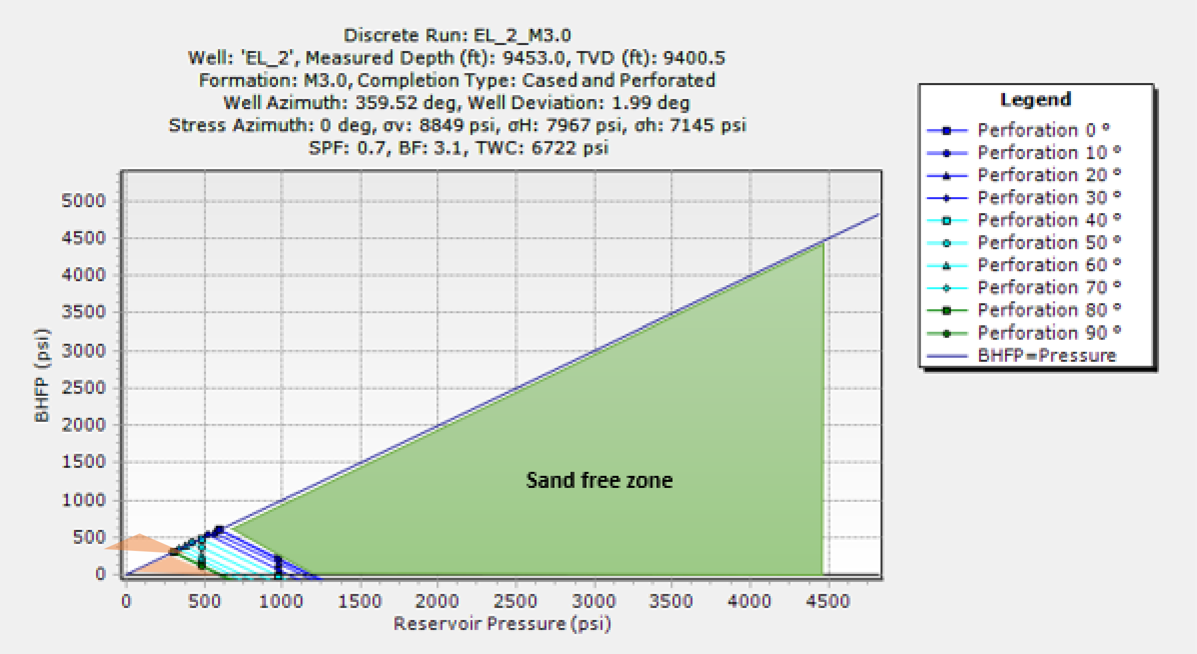

Figure 17: CDP prediction using shear failure model for perforated well EL 2 (Reservoir M3.0)

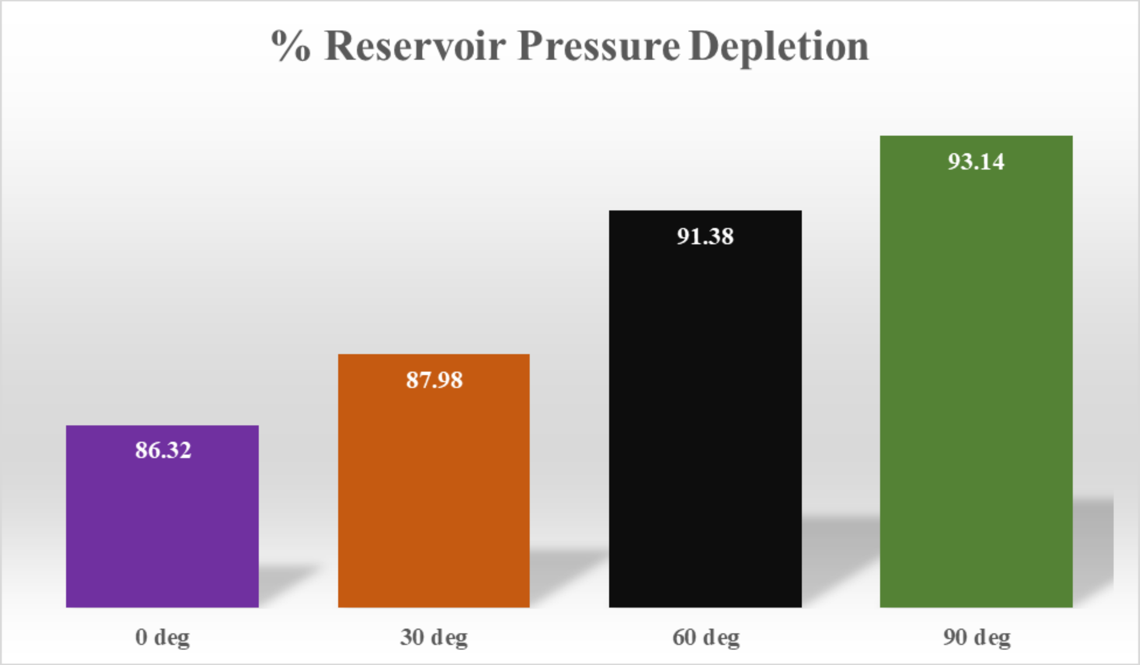

Figure 18: Histogram plot of percentage reservoir pressure depletion before the onset of sand production for Reservoir M3.0

Table 6a: Result for sand control technique

Sample ID	D_{10} (mm)	D_{40} (mm)	D_{90} (mm)	D_{95} (mm)	SC	UC	Fines (<44 µm) (%)	D_{50} (mm)	Sand control Technique
K7.1	1.16	0.32	0.070	0.059	19.66	4.57	0.98	0.25	Gravel pack
L9.1	1.18	0.26	0.064	0.060	19.67	4.06	2.00	0.20	Gravel Pack
M1.0	1.23	0.20	0.066	0.062	19.84	3.03	1.40	0.15	Gravel pack
M3.0	0.45	0.18	0.072	0.065	6.92	2.50	1.20	0.15	SAS (wire wrapped screen)

Table 6b: Result for estimated Gravel size, screen size and screen slot size for gravel pack and Standalone Screen (SAS)

Reservoir	Largest gravel size (mm)	Smallest gravel size (mm)	Selected Gravel Mesh Size	Screen size (micron)	Screen slot size for SAS – D30 (micron)
K7.1	2	1	12/20 US Mesh	500	-
L9.1	1.16	0.8	12/20 US Mesh	400	-
M1.0	1.12	0.6	20/40 US Mesh	300	-
M3.0	1.12	0.6	20/40 US Mesh	300	200

Figure 19 shows the sieve curve for K7.1. The curve was used to deduce D10 , D40, D50, D90, D95. From these percentiles, sorting coefficient (SC) and uniformity coefficient (UC) are estimated to be 19.66 and 4.57 respectively and fines content of about 0.98% (Table 6a). Based on this, it is observed that the sample SC<20, UC<5 and fines content <5% Therefore, from table 7, it is observed that the optimum sand control technique for K7.1 is Gravel Pack with the largest and smallest gravel sizes of 2mm and 1mm respectively. However, the smallest gravel size fit into 12/20 US mesh and a screen size of 500 micron (Table 6b).

For reservoir L9.1, the PSD curve (Figure 20) was also used obtain the appropriate percentiles for the evaluation. From Table 6a, the sorting coefficient (SC) was calculated as 19.67 and the uniformity coefficient (UC) as 4.06, while the fines content was about 2%. Since these values meet the conditions of SC below 20, UC less than 5, and fines content under 5%, the most suitable sand control method is a Gravel Pack. The recommended gravel sizes range from 0.8 mm to 1.16 mm, which aligns with a 12/20 US mesh, and the corresponding screen size is 400 µm (Table 6b).

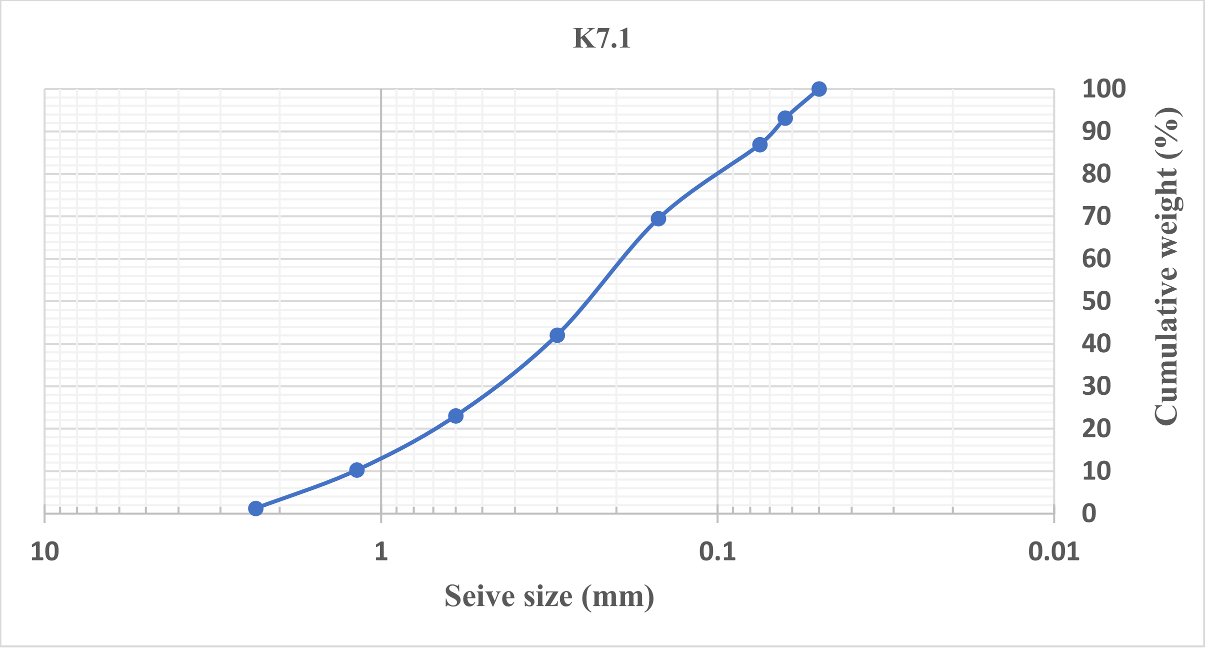

Figure 19: Particle Size Distribution (PSD) curve for K7.1 showing the cumulative distribution of particle sizes within the sample

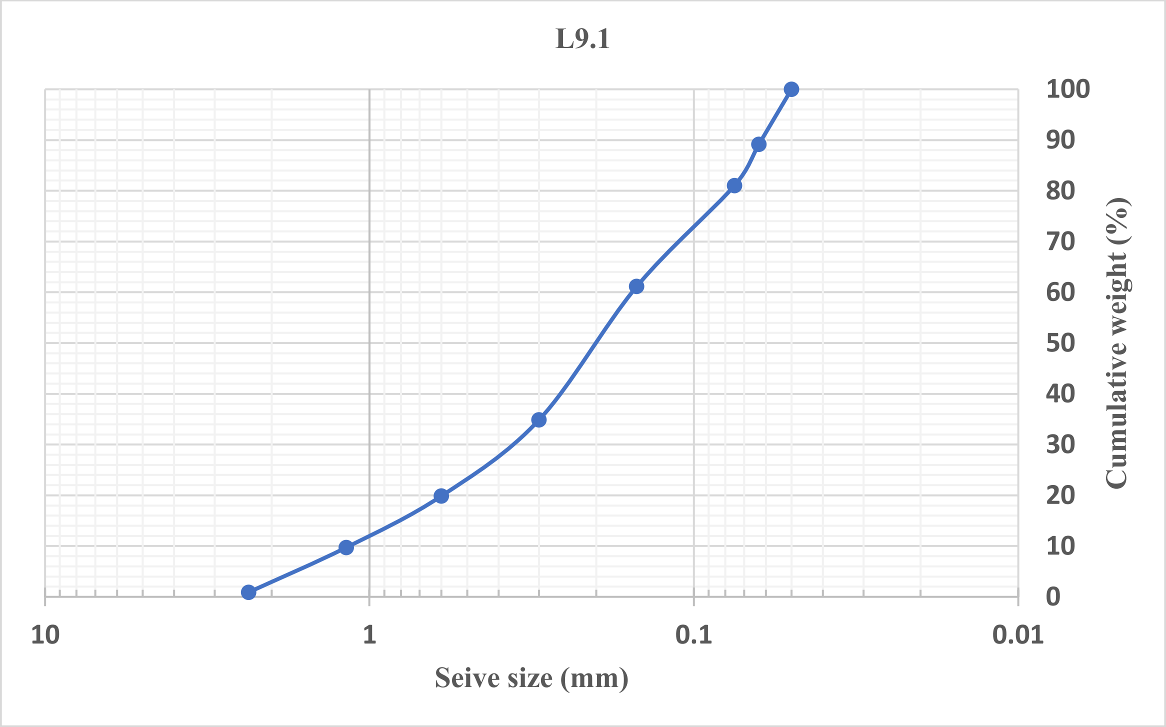

Figure 20: PSD curve for L9.1

In the case of reservoir M1.0, sieve analysis (Figure 21) was employed to obtain D10, D40, D50, D90, and D95 values. Using these parameters, the sorting coefficient (SC) is 19.84, while the uniformity coefficient (UC) is 3.03, with fines content measuring approximately 1.4% (Table 6a). Since the results fall within the criteria of SC less than 20, UC below 5, and fines content under 5%, a Gravel Pack is considered the most effective sand control approach. The selected gravel size ranges between 0.6 mm and 1.12 mm, which corresponds to a 20/40 US mesh, and the appropriate screen size for the completion is 300 µm (Table 6b).

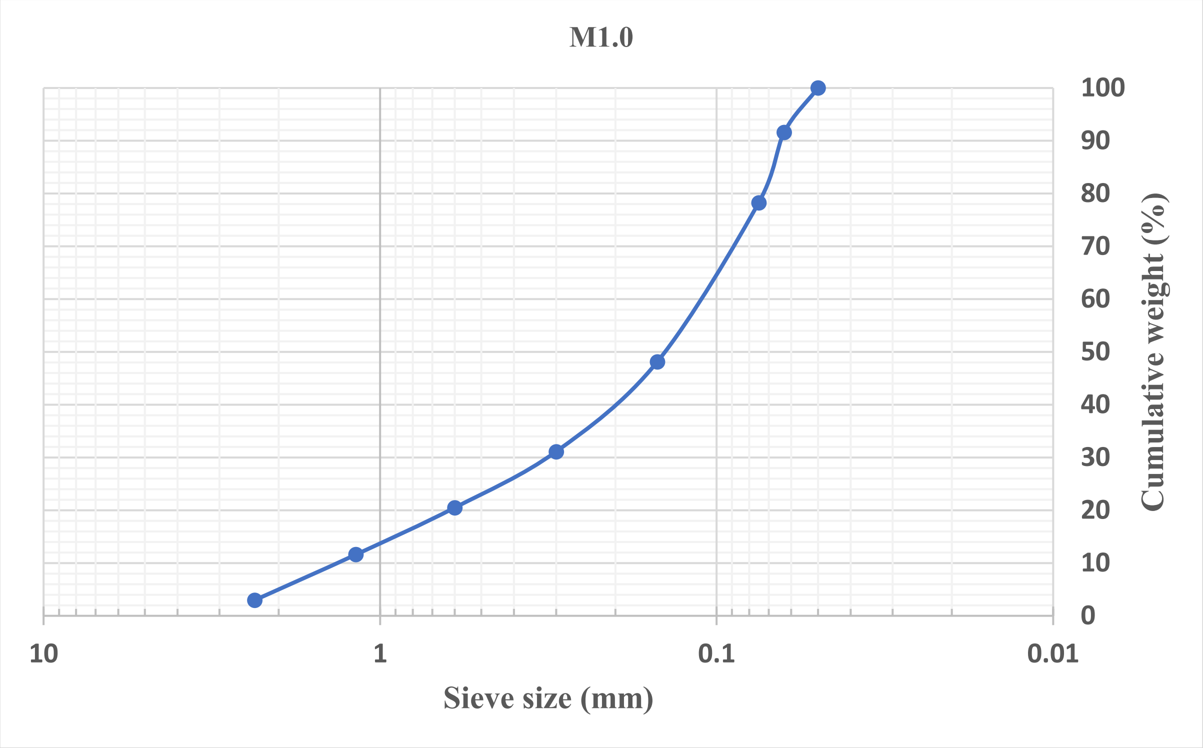

Figure 21: PSD curve for M1.0

For reservoir M3.0, the sieve analysis (Figure 22) was also used to determine D10, D40, D50, D90, and D95 values. From these, the sorting coefficient (SC) and uniformity coefficient (UC) are 6.92 and 2.5, respectively, with fines content of about 1.2% (Table 6a). Since the values satisfy the criteria of SC <10, UC <3, and fines <2%, the most suitable sand control option is a Standalone Screen (wire-wrapped screen). The recommended gravel sizes range between 0.6 mm and 1.12 mm, corresponding to a 20/40 US mesh. In addition, the appropriate screen slot size for the SAS is selected at D30 (200 µm), with a screen size of 300 µm (Table 6b).

5.0 Discussion

The results of average elastic properties of the four studied reservoirs (K7.1, L9.1, M1.0, and M3.0) fall within the typical ranges reported for consolidated to moderately consolidated sandstones in the Niger Delta Basin (Zoback, 2010; Afolayan et al., 2024), suggesting moderately stiff and moderately compressible clastic rock frameworks. The K7.1 Reservoir records the lowest elastic stiffness among the studied intervals. Its relatively high Biot coefficient reflects strong poroelastic sensitivity, indicating that pore pressure variations exert significant control on effective stress. This mechanical behavior is consistent with recent Niger Delta studies that associate shallow reservoir sands with weaker grain frameworks, higher clay content, and limited cementation, resulting in lower elastic moduli and higher susceptibility to deformation (Eze et al., 2023; Oladapo et al., 2024). Similar elastic ranges have been reported for shallow unconsolidated sands in several Niger Delta fields, reinforcing the interpretation of K7.1 as mechanically weak and sand-prone (Afolayan et al., 2024). The L9.1 Reservoir exhibits intermediate stiffness as its elastic properties reflect a transitional mechanical regime between the shallow K7.1 sands and the deeper M-series reservoirs. Comparable elastic trends have been documented in recent Niger Delta geomechanical studies, where progressive burial depth and compaction result in moderate increases in stiffness and reduced poroelastic sensitivity (Nwozor et al., 2024).

Such transitional reservoirs are often identified as conditionally stable, requiring controlled drawdown and optimized completion design to mitigate sanding risk (Osisanya & Ojo, 2023). The M1.0 Reservoir shows the highest average stiffness and its Biot coefficient indicates reduced pore pressure sensitivity and a strong load-bearing grain framework.

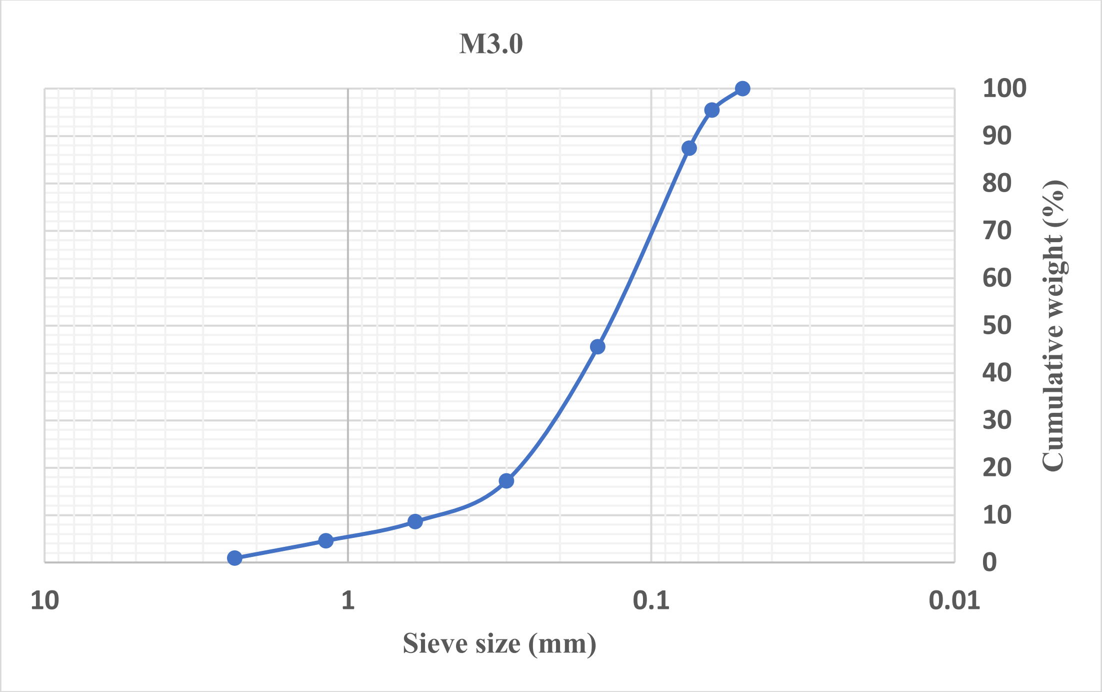

Figure 22: PSD curve for M3.0

Furthermore, the properties closely align with recent log-derived geomechanical studies in deeper well-compacted and cemented sandstones Niger Delta reservoirs (Afolayan et al., 2024; Nwozor et al., 2024). Such reservoirs are generally characterized by higher mechanical stability and greater resistance to sanding onset. The M3.0 Reservoir exhibits similar elastic behavior to M1.0, albeit with slightly lower stiffness These properties are consistent with elastic ranges reported for deeply buried Niger Delta sandstones that have undergone significant compaction and diagenetic cementation, resulting in stiff and relatively incompressible formations (Eze et al., 2023; Oladapo et al., 2024). Overall, a clear depth-dependent mechanical trend is observed across the reservoirs, following the sequence K7.1 < L9.1 < M1.0 < M3.0 in terms of stiffness and decreasing poroelastic sensitivity. This trend mirrors basin-wide compaction patterns documented in recent Niger Delta studies, where increasing burial depth leads to enhanced cementation, reduced porosity, and improved mechanical competence (Afolayan et al., 2024; Nwozor et al., 2024). The consistency between the present results and regional studies lends confidence to the reliability of the log-derived elastic properties. From a sand management perspective, the M-series reservoirs (M1.0 and M3.0) are mechanically robust and capable of sustaining higher drawdowns before the onset of mechanical failure. However, similar to observations in other deep Niger Delta reservoirs, once failure is initiated, these stiff formations may release larger volumes of sand due to the accumulation of higher elastic strain energy prior to failure (Morita et al., 1989a; Schutjens et al., 2023). In contrast, the K7.1 Reservoir is mechanically weaker, more sensitive to pore pressure depletion, and thus more prone to early sanding during production. The L9.1 Reservoir represents an intermediate case, where effective drawdown management and stress-aligned perforation strategies are critical for maintaining stable production, as demonstrated in recent Niger Delta field applications (Osisanya & Ojo, 2023; Wang et al., 2024). It is important to note that uncertainties remain due to the reliance on dynamic elastic properties derived from sonic logs, which are known to overestimate stiffness relative to static laboratory measurements. This limitation has been widely recognized in Niger Delta geomechanical studies, and the application of empirical dynamic-to-static correction factors is recommended to improve prediction reliability (Fjær et al., 2023).

The rock strength properties of the four studied reservoirs (K7.1, L9.1, M1.0, and M3.0) were assessed using UCS, cohesion, tensile strength, and friction angle to evaluate sanding potential under varying stress and drawdown conditions, consistent with recent Niger Delta studies (Adewole & Olafuyi, 2019; Olatunji et al., 2021). K7.1 exhibits the lowest strength, indicating weak intergranular bonding, low tensile resistance, and high susceptibility to shear failure and early-life sanding under modest drawdown, in line with observations for shallow Niger Delta sands (Adebayo et al., 2018; Adeyanju & Olayinka, 2020). L9.1 shows intermediate UCS, cohesion, and tensile strength, reflecting improved cementation and compaction, with moderate friction angles that support stability under controlled drawdown but potential sanding with depletion (Olatunji et al., 2021; Okorie et al., 2022). M1.0 represents the strongest interval, with high UCS, cohesion, and friction angle, indicating robust resistance to sand detachment even at higher production rates (Adewole & Olafuyi, 2019; Akinwale et al., 2023). M3.0 is slightly weaker than M1.0 but remains mechanically strong, capable of sustaining drawdown safely, with sanding typically localized near perforations or weak planes (Okorie et al., 2022). Overall, sanding susceptibility decreases with increasing rock strength, with K7.1 being most at risk, M-series sands exhibiting higher tolerance, and L9.1 requiring careful monitoring, consistent with documented Niger Delta sand production behavior where mechanical strength, stress path, and production strategy collectively govern sanding risk (Adebayo et al., 2018; Akinwale et al., 2023).

The in-situ stress regime of the studied reservoirs (K7.1, L9.1, M1.0, and M3.0) was characterized by vertical stress (σv), minimum and maximum horizontal stresses (Shmin and SHmax), and pore pressure (Pp), which are fundamental for assessing wellbore stability and sand failure, as widely applied in Niger Delta geomechanical studies (Zoback, 2010; Adewole & Olafuyi, 2019). In all reservoirs, horizontal stresses are consistently lower than vertical stress, indicating a transition from normal faulting to strike-slip conditions typical of the Niger Delta, influenced by sediment loading, shale compaction, and regional tectonic relaxation (Akinwale et al., 2020; Olatunji et al., 2021). Pore pressure increases systematically with depth due to compaction-driven overpressure, a common feature in deltaic depobelts (Bowers, 1995; Adeyanju & Olayinka, 2020). K7.1 exhibits the lowest stress magnitudes and high Biot coefficient, making it highly sensitive to pore pressure changes and prone to sanding under modest drawdown, consistent with shallow Niger Delta reservoirs exhibiting high poroelastic sensitivity (Adebayo et al., 2018; Okorie et al., 2022). L9.1 shows intermediate stress magnitudes and moderate Biot sensitivity, allowing greater tolerance to stress changes than K7.1 but still requiring monitoring for localized stress concentrations and depletion effects, as reported for mid-depth reservoirs (Olatunji et al., 2021). M1.0 is characterized by higher stress magnitudes and reduced Biot sensitivity, reflecting its deeper burial and stronger elastic framework, which, together with higher UCS and cohesion, enhances stability under drawdown; similar stress–strength relationships are observed in deeper Niger Delta reservoirs where sanding occurs primarily under extreme drawdown or around perforations (Adewole & Olafuyi, 2019; Akinwale et al., 2023). M3.0 exhibits a stress profile comparable to M1.0, with limited poroelastic coupling and high strength, demonstrating robust mechanical stability, although localized sanding can occur if drawdown is not carefully managed, consistent with recent observations of deep Niger Delta reservoirs (Okorie et al., 2022; Akinwale et al., 2023).

Elastic parameters serve as an effective first-order tool for evaluating reservoir sanding potential. In this study, three indices i.e. the Sand Production Index (B) (Dong et al., 2013), the shear modulus to bulk compressibility ratio (J) (Tixier, 1975), and the Schlumberger Sand Production Index (SI) (Bianlong et al., 2013), were applied to assess sanding susceptibility across the four reservoirs. These indices remain widely used in recent Niger Delta and global studies for rapid sanding risk screening (Akinwale et al., 2023; Osisanya et al., 2023; Zhang et al., 2024). The applied thresholds were 2.9 Mpsi^2 for B-index, 0.8×10^6 Mpsi^2 for J, and 1.24×10^6 Mpsi^2 for SI, with values below the cutoff indicating potential sand production, consistent with recent elastic screening practices that integrate stress and strength considerations (Adebayo et al., 2024; Silva et al., 2023). K7.1 exhibits a B-index well below the threshold, suggesting high sanding risk, though its SI and J values are above cutoffs, reflecting the conservative nature of the B-index in identifying weakly consolidated sands, as observed in shallow Niger Delta reservoirs (Osisanya et al., 2023; Akinwale et al., 2023; Zhang et al., 2024). L9.1 shows an intermediate mechanical response, with the B-index below the threshold but SI and J above, demonstrating that mid-depth reservoirs may display mixed classifications requiring complementary stress and strength analysis (Adebayo et al., 2024; Osisanya et al., 2023). The deeper reservoirs, M1.0 and M3.0, exceed all three thresholds, consistently indicating mechanical stability, in agreement with their high stiffness, compaction, and diagenetic consolidation; similar trends have been reported for deep Niger Delta and offshore Brazil reservoirs (Silva et al., 2023; Akinwale et al., 2023; Zhang et al., 2024). Overall, the B-index identifies the shallower reservoirs (K7.1 and L9.1) as more prone to sanding, while the deeper M-series reservoirs show stability, stressing the importance of integrating elastic-based screening with stress-path and rock strength analyses for accurate sand risk prediction (Adebayo et al., 2024; Zhang et al., 2024).

The shear failure model of Critical Drawdown Pressure (CDP), Bottomhole Flowing Pressure (BHFP), and failure pressures across the four reservoirs demonstrates clear contrasts in sanding behavior that are strongly controlled by reservoir depth, mechanical competence, and perforation orientation. The shallow K7.1 reservoir shows a strong tendency for early sand onset, reflecting the behavior of weakly consolidated Niger Delta sands that are highly sensitive to modest drawdown and poroelastic stress changes (Adebayo et al., 2018; Adeyanju & Olayinka, 2020). In contrast, L9.1 exhibits greater tolerance to depletion before sanding, consistent with mid-depth Niger Delta reservoirs where improved compaction and cementation delay failure but do not eliminate sanding risk (Olatunji et al., 2021; Okorie et al., 2022). The deeper M-series reservoirs (M1.0 and M3.0) display substantially higher resilience to depletion, with sanding largely delayed to advanced stages of production, reflecting their stronger mechanical framework. However, the results also indicate that once failure is initiated in these deeper sands, sand production may be abrupt and severe, a behavior widely reported in compacted clastic reservoirs both within and outside the Niger Delta (Adewole & Olafuyi, 2019; Silva et al., 2023). Across all reservoirs, perforation orientation plays a critical role, with higher-angle perforations generally enhancing resistance to shear failure and delaying sanding onset, in agreement with established geomechanical principles and recent regional and global studies (Akinwale et al., 2023; Zhang et al., 2024). Overall, the results buttress that sand management strategies must be reservoir-specific, integrating drawdown control, perforation design, and appropriate completion choices to effectively mitigate sanding in unconsolidated and weakly consolidated reservoirs.

The selection of sand control techniques for reservoirs K7.1, L9.1, M1.0, and M3.0 was guided by grain size distribution, sorting coefficient (SC), uniformity coefficient (UC), and fines content, which remain the foundation of classical and modern sand control design (Coberly, 1937; Saucier, 1974). The results indicate that sand control effectiveness is strongly reservoir-specific, with broader grain size distributions, poorer sorting, and higher fines content requiring more robust sand retention systems, while well-sorted formations with limited fines can be completed using less restrictive solutions without compromising performance (Akinwale et al., 2023; Osisanya et al., 2023). Accordingly, gravel pack completion is recommended for reservoirs K7.1, L9.1, and M1.0 due to their grain size characteristics and fines content, consistent with recent field and modeling studies that demonstrate superior gravel pack performance in moderately to poorly sorted sands (Adebayo et al., 2024; Al-Awadhi et al., 2024). In contrast, reservoir M3.0 is suitable for a standalone screen, as its favorable sorting and lower fines content support effective sand exclusion while preserving productivity, in agreement with observations from well-sorted clastic reservoirs (Silva et al., 2023). Overall, the adopted reservoir-specific, data-driven sand control framework aligns with established design methodologies and recent best practices, optimizing sand retention, minimizing productivity impairment, and supporting sustainable long-term reservoir development (Zhang et al., 2025).

5.0 Conclusions

This study focused on the evaluation of sanding potential in the EL Field, Niger Delta, with the aim of generating geomechanical results that can guide reservoir management and completion design. The study utilized available well log data, empirical correlations, and sieve analysis of ditch cuttings to estimate elastic and strength properties, assess sanding risk through multiple approaches, and provide practical recommendations for sand control.

The results indicate that the shallower reservoirs, particularly K7.1 and L9.1, are mechanically weaker, characterized by low Young's modulus, low unconfined compressive strength, and high compressibility. These properties render them highly susceptible to sanding during production. In contrast, the deeper M-series reservoirs (M1.0 and M3.0) exhibit higher stiffness and strength, resulting in greater stability and lower sanding risk.

Sanding potential assessment using the Sand Production Index (B), Schlumberger Sand Index (SI), and G/CB ratio provided consistent results, all pointing to high sanding risk in the shallow reservoirs and lower risk in the deeper sands. Critical Drawdown Pressure (CDP) analysis further validated these trends, showing that sanding onset occurs at relatively low drawdowns in the shallow reservoirs, while the deeper intervals can sustain much higher drawdowns before failure. Importantly, the CDP analysis also emphasized the role of perforation orientation, with 60–90° perforations demonstrating the greatest resistance to sanding compared to lower perforation orientations.

The sieve analysis of ditch cuttings provided an additional layer of evaluation by quantifying particle size distribution, fines content, and sorting characteristics. These results were used to guide sand control completion design. For the shallow sanding-prone units, gravel packing was identified as the most suitable completion option. Conversely, for the deeper and more competent reservoirs, stand-alone screens may be sufficient, provided that production is carefully managed within the safe drawdown limits established by the CDP results.

Despite these results, the study has some limitations. The geomechanical properties were largely derived from well log–based empirical correlations, which inherently assume homogeneous lithology and may not fully capture local heterogeneities, cementation variations, or anisotropy. In addition, the absence of core-based laboratory measurements limited direct calibration of the estimated elastic and strength parameters, introducing uncertainty into the absolute magnitudes of sanding thresholds and CDP values. The use of ditch cuttings, while practical, may also underrepresent in-situ grain fabric and fines migration behavior under dynamic flow conditions.

Future research should therefore focus on integrating core-derived mechanical testing and triaxial laboratory experiments to calibrate and refine log-based estimates. Time-lapse (4D) geomechanical modeling that incorporates depletion-induced stress path evolution would further improve sanding predictions, particularly for long-term production planning. In addition, coupling geomechanical models with production data and real-time sand monitoring would enable validation of predicted sanding onset and enhance adaptive sand management strategies. Such integrated approaches would strengthen the reliability of sanding risk prediction and support more robust completion and production optimization in the EL Field and similar Niger Delta reservoirs.

Acknowledgements

The dataset utilized in this study was provided by Heritage Energy Operational Services Limited (HEOSL) on behalf of the Nigerian Petroleum Development Company (NPDC) and Shoreline Natural Resources., for which the first author is quite appreciative.

References

Abdideh, M., Rashidi, S., & Khamehchi, E. (2023). Sand production prediction using coupled geomechanical and reservoir simulation approaches. *Journal of Petroleum Science and Engineering, 223*, 111374. https://doi.org/10.1016/j.petrol.2023.111374

Abija, F.A. & Tse, A, C. (2016). Geomechanical evaluation of an onshore oil field in the Niger Delta, Nigeria. *Journal of Applied Geology and Geophysics,* 4(1). pp.99111.

Adebayo, A. R., Orodu, O. D., & Dada, S. A. (2018). Geomechanical characterization and sand production prediction in unconsolidated Niger Delta reservoirs. *Journal of Petroleum Exploration and Production Technology, 8*(4), 1197–1210. https://doi.org/10.1007/s13202-018-0465-2

Adebayo, A. R., Orodu, O. D., & Dada, S. A. (2024). Integrated elastic and geomechanical screening of sand production risk in Niger Delta reservoirs. *Journal of Petroleum Science and Engineering, 233*, 112368.

Adewole, E. S., & Olafuyi, O. A. (2019). Evaluation of in-situ stress and sanding potential in Niger Delta reservoirs. *Journal of Petroleum Science and Engineering, 173*, 849–860.

Adewole, O., Olatunji, A., & Lawal, K. (2023). Integrated geomechanical assessment for sand production prediction in unconsolidated sandstone reservoirs. *Journal of Petroleum Science and Engineering, 228*, 111879. https://doi.org/10.1016/j.petrol.2023.111879.

Adeyanju, O. A. & Oyekunle, L. O. (2020). Sand production challenges in Niger Delta oil fields: Causes, consequences, and control measures. *Journal of Petroleum Engineering*, *45*(2), 135-152.

Afolayan, J. O., Ojo, A. O. & Adebola, O. O. (2024). Log-based geomechanical modeling for sanding risk assessment in Niger Delta reservoirs. *Petroleum Research, 9*(2), 185–198. https://doi.org/10.1016/j.ptlrs.2024.02.006.

Ahmed, U., Markley, M.E. & Crary, S.F. (1991). Enhanced in-situ stress profiling with micro fracture, core and sonic logging data. *SPE Form. Eval*. 6(02). 243-251.

Akinwale, A. A., Olatunji, S. O. & Adepoju, O. O. (2023). Coupled stress–pore pressure effects on sanding in Niger Delta reservoirs. *Journal of Petroleum Science and Engineering, 221*, 111242.

Akinwale, A. A., Olatunji, S. O. & Adepoju, O. O. (2023). Influence of rock strength parameters on sand production under increasing drawdown in Niger Delta reservoirs. *Journal of Petroleum Science and Engineering, 221*, 111242.

Akinwale, A. A., Olatunji, S. O. & Lawal, K. A. (2020). Stress regime characterization and its implication for wellbore stability in the Niger Delta. *Journal of African Earth Sciences, 167*, 103853.

Azizi, H., & Memarian, H. (2015). Application of log-derived geomechanical properties to sand production prediction. *Journal of Petroleum Exploration and Production Technology, 5*(3), 225–236.

Bianlong, L., Jun, Y. & Ming, Z. (2013). Evaluation of sand production using elastic parameters. *Petroleum Exploration and Development, 40*(5), 639–646.

Chen, Z., Liu, H. & Wu, X. (2024). Numerical investigation of sand onset mechanisms in weakly cemented sandstone reservoirs. *Rock Mechanics and Rock Engineering, 57*, 2141–2159. https://doi.org/10.1007/s00603-024-03412-7

Damuth, J. E. (1994). Neogene gravity tectonics and depositional processes on the deep Niger Delta continental margin. *Marine and Petroleum Geology*, 11(3), 320–346.

Ding, W., Zhou, H. & Wang, S. (2018). Advances in sand control techniques: An integrated geomechanical approach. *Journal of Natural Gas Science and Engineering*, *51*, 312-328.

Dong, C., Li, X. & Liu, J. (2013). A new elastic modulus-based sand production index. *Journal of Petroleum Science and Engineering, 103*, 1–8.

Doust, H. & Omatsola, E. (1990). Niger Delta. In J. D. Edwards & P. A. Santogrossi (Eds.), *Divergent/passive margin basins* (Vol. 48, pp. 201–238). AAPG Memoir.

Eshkalak, M. O., Mohaghegh, S. D. & Esmaili, S. (2014). Geomechanical properties of unconventional shale reservoirs. *Journal of Petroleum Engineering*, 2014, Article ID 961641. https://doi.org/10.1155/2014/961641

Evamy, B. D., Haremboure, J., Kamerling, P., Knaap, W. A., Molloy, F. A. & Rowlands, P. H. (1978). Hydrocarbon habitat of Tertiary Niger Delta. *AAPG Bulletin, 62*(1), 1–39.

Eze, C. L., Nwankwo, C. N. & Okorie, P. E. (2023). Evaluation of sanding potential using elastic properties derived from wireline logs in Niger Delta reservoirs. *Journal of African Earth Sciences, 198*, 104828. https://doi.org/10.1016/j.jafrearsci.2023.104828

Fjær, E., Holt, R. M., Horsrud, P., Raaen, A. M. & Risnes, R. (2023). *Petroleum related rock mechanics* (3rd ed.). Elsevier.

Genik, G. J. (1993). Petroleum geology of Cretaceous-Tertiary rift basins in Niger, Chad, and Central African Republic. *AAPG Bulletin*, 77(8), 1405–1434.

Holbrook, P.W. & Maggiori D.A. (1993). Real time pore pressure and fracture gradient evaluation in all sedimentary lithologies. In: *Proceedings of Offshore European Conference. Aberdeen, Scotland, SPE*: 1993. Paper SPE 26791.

Jones M.E., Leddra, M.J., Goldsmith, A.S. & Edwards, D. (1992). The Geomechanical Characteristics of Reservoirs and Reservoir Rocks, Health and Safety Executive - Offshore Technology Report. London: HMSO Books.

Khaksar, A., Geilikman, M. & Ding, Y. (2024). Advances in sand control technology for unconsolidated reservoirs. *SPE Production & Operations, 39*(1), 67–82. https://doi.org/10.2118/218203-PA

Khaksar, A., Taylor, P. G., Fang, Z., Kayes, T. J. & Rahman, K. (2009). Rock strength from core and logs: Where we stand and ways to go. *Proceedings of the SPE EUROPEC/EAGE Conference and Exhibition*. https://doi.org/10.2118/121972-MS

Kidambi, T. & Kumar, G.S. (2016). Mechanical earth modeling for a vertical well drilled in a nationally fracture light carbonate gas reservoir in the *Persian Gulf. Journal of Petro. Sci. Eng., 141, 38-51.*

Maleki, S., Moradzadeh, A., Riabi, R.G. & Sadaghzadeh, F. (2014). Comparison of several different methods of in situ stress determination. *International Journal of Rocks Mechanics and Mining Science*. 7, 395-404.

McNally, C. (1999). *Predicting sand production in weak reservoir formations*. Journal of Petroleum Technology, 51(6), 72–78.

Morita, N., Whitfill, D. L., Fedde, R. D., & Vaziri, H. (1989a). Parametric study of sanding prediction: Analytical approach. *SPE Drilling Engineering*, 4(1), 41–49.

Morita, N., Whitfill, D. L., Massie, I. & Knudsen, T. W. (1989b). Realistic sand production prediction. *SPE Production Engineering, 4*(1), 15–24. https://doi.org/10.2118/16989-PA

Morley, C. K. (2009). Geometry and evolution of large-scale normal faults in sedimentary basins: Insights from gravity-driven deformation in the Niger Delta. *Marine and Petroleum Geology, 26*(9), 1459–1475. https://doi.org/10.1016/j.marpetgeo.2009.02.004.

Nwozor, K. K., Onyekuru, S. O. & Omudu, L. M. (2024). Reservoir depletion and stress-path effects on sand production in deltaic environments. *Marine and Petroleum Geology, 158*, 106603. https://doi.org/10.1016/j.marpetgeo.2023.106603

Oil and Natural Gas Corporation Limited. (2018). Sand control in Lakwa Field of Assam Asset, Pages 8-28, Institute of

Oil and Gas Production Technology, Panvel, Navi Mumbai.

Okorie, P. E., Onyekachi, N. C. & Ugwu, S. A. (2022). Stress evolution and sanding risk assessment in depleted Niger Delta reservoirs. *SPE Nigeria Annual International Conference and Exhibition*. https://doi.org/10.2118-/209201-MS.

Oladapo, A. O., Bello, O. S. & Adebayo, A. R. (2024). Sand production challenges and mitigation strategies in mature Niger Delta fields. *Journal of African Earth Sciences, 206*, 105021. https://doi.org/-10.1016/j.jafrearsci.2024.105021.

Olatunji, S. O., Akinwale, A. A. & Lawal, K. A. (2021). Integrated geomechanical modeling for sand management in Niger Delta oil fields. *Journal of African Earth Sciences, 181*, 104249.

Omar, I. (2015). Reservoir geomechanics lecture slides. Stanford University. Available from: *https://lagunita.Stanford.edu-./Course v1…about.*

Osisanya, O., Adeola, T. O. & Bello, R. S. (2023a). Evaluation of formation susceptibility and sand production potential in an offshore Niger Delta field. *Energy Geoscience,* 5(1), 100213.

Osisanya, S. O. (2021). Sanding mechanisms and critical drawdown pressure analysis in weakly consolidated formations. *SPE Journal, 26*(2), 911–926. https://doi.org/10.2118/203684-PA

Osisanya, S. O. & Ojo, A. O. (2023b). Critical drawdown pressure modeling for sanding prediction in weakly consolidated reservoirs. *SPE Journal, 28*(3), 1325–1340. https://doi.org/10.2-118/215442-PA.

Ostadhassan, M., Zong, Z. & Zamrian, S. (2012). Geomechanical modeling of an anisotropic formation-Bakken: Case study. 46th US Rock Mechanics/ Geomechanics Symposium American Rock Mechanics Association.

Plumb, R., Edwards, S., Pidcock, G., Lee, D. & Stacey, B. (2000). The mechanical earth model concept and its application. *SPE Reservoir Evaluation & Engineering, 3*(2), 165–179. https://-doi.org/10.2118/59128-PA.

Reijers, T. J. A. (2011). Stratigraphy and sedimentology of the Niger Delta. *Geologos*, 17(3), 133–162.

Santarelli, F. J., Rojas, J. C. & Fullmer, S. (2020). Sand production mechanisms and geomechanical controls. *International Journal of Rock Mechanics and Mining Sciences*, *74*, 98-112.

Sayers, C. M. & Zoback, M. D. (2023). Reservoir geomechanics for sand production and well integrity. *Annual Review of Earth and Planetary Sciences, 51*, 489–514. https://doi.org-/10.1146/annurev-earth-032320-082404

Schlumberger, (1985). *Well Evaluation Conference*. Nigeria.

Schutjens, P., Sayers, C. M. & Zoback, M. D. (2023). Sanding prediction using coupled geomechanical and production models. *SPE Production & Operations, 38*(4), 821–835. https://doi.org/-10.2118/214801-PA.

Seyed, S. S. & Aghighi, M.A. (2015). Building and analyzing geomechanical model of Bangestan reservoir in Kopal oil field, Iranian. *Journal of Mining Engineering*, 10, 21-34.

Short, K. C. & Stauble, A. J. (1967). Outline of geology of Niger Delta. *AAPG Bulletin*, 51(5), 761–779.

Silva, R. F., Almeida, L. P. & Santos, J. M. (2023). Elastic property-based sand production screening in deepwater turbidite reservoirs, offshore Brazil. *Journal of Petroleum Science and Engineering, 226*, 111730.

Tixier, M. P. (1975). Mechanical properties of reservoir rocks. *Journal of Petroleum Technology, 27*(2), 237–244.

Udegbunam, E. O., Adekanle, A. O. & Alao, O. O. (2025). Integrated sanding prediction using critical drawdown pressure and perforation orientation analysis. *Journal of Natural Gas Science and Engineering, 116*, 105223. https://doi.org/10.1016/j.jngse.2024.105223.

Van den Hoek, P. J. & Geilikman, M. (2023). Screen selection and completion optimization based on sanding severity indices. *SPE Drilling & Completion, 38*(3), 451–466. https://doi.org/10.2118/216489-PA.

Veeken, C. A. M., Davies, D. R., Kenter, C. J. & Kooijman, A. P. (1991). Sand production prediction review: Developing an integrated approach. *SPE Annual Technical Conference and Exhibition*.

Wang, J., Ma, T. & Chen, P. (2024). Effect of perforation geometry and orientation on sand production in unconsolidated formations. *Journal of Petroleum Science and Engineering, 231*, 112074. https://doi.org/10.1016/j.petrol.2024.112074

Whiteman, A. (1982). *Nigeria: Its Petroleum Geology, Resources and Potential* (Vol. 1 & 2). London: Graham and Trotman.

Zhang, J. (2013a). Effective stress and sand production in weakly cemented formations: A geomechanical perspective. *Journal of Petroleum Science and Engineering*, *105*, 32-44.

Zhang, J. (2013b). Borehole stability analysis accounting for anisotropic stress and depletion effects. *Journal of Petroleum Science and Engineering, 110*, 260–272. https://doi.org/10.1016/j.petrol-.2013.08.035.

Zhang, Y., Liu, H., Sun, L. & Wang, Q. (2024). Elastic parameter sensitivity and sand production prediction in clastic reservoirs under depletion. *Engineering Geology, 332*, 107395.

Zoback, M. D. (2010). *Reservoir geomechanics*. Cambridge University Press.